SANDIA REPORT

SAND2003-0723
Unlimited Release
Printed March 2003

Innovative Design Approaches for Large Wind Turbine Blades

TPI Composites, Inc.
373 Market Street
Warren, RI 02885

Prepared by
Sandia National Laboratories
Albuquerque, New Mexico 87185 and Livermore, California 94550

Sandia is a multiprogram laboratory operated by Sandia Corporation,
a Lockheed Martin Company, for the United States Department of Energy's
National Nuclear Security Administration under Contract DE-AC04-94AL85000.

Issued by Sandia National Laboratories, operated for the United States Department of Energy by Sandia Corporation.

Available to DOE and DOE contractors from
U.S. Department of Energy
Office of Scientific and Technical Information
P.O. Box 62
Oak Ridge, TN 37831

Telephone: (865)576-8401
Facsimile: (865)576-5728
E-Mail: reports@adonis.osti.gov
Online ordering: http://www.doe.gov/bridge

Available to the public from
U.S. Department of Commerce
National Technical Information Service
5285 Port Royal Rd
Springfield, VA 22161

Telephone: (800)553-6847
Facsimile: (703)605-6900
E-Mail: orders@ntis.fedworld.gov
Online order: http://www.ntis.gov/help/ordermethods.asp?loc=7-4-0#online

SAND 2003-0723
Unlimited Release
Printed March 2003

INNOVATIVE DESIGN APPROACHES FOR LARGE WIND TURBINE BLADES

WindPACT Blade System Design Studies

TPI Composites, Inc.
373 Market Street
Warren, RI

ABSTRACT

The primary goal of the WindPACT Blade System Design Study (BSDS) was investigation and evaluation of design and manufacturing issues for wind turbine blades in the one to ten megawatt size range. The initial project task was to assess the fundamental physical and manufacturing issues that govern and constrain large blades and entails three basic elements: 1) a parametric scaling study to assess blade structure using current technology, 2) an economic study of the cost to manufacture, transport, and install large blades, and 3) identification of promising innovative design approaches that show potential for overcoming fundamental physical and manufacturing constraints.

This report discusses several innovative design approaches and their potential for blade cost reduction. During this effort we reviewed methods for optimizing the blade cross-section to improve structural and manufacturing characteristics. We also analyzed and compared a number of composite materials and evaluated their relative merits for use in large wind turbine blades in the range from 30 meters to 70 meters. The results have been summarized in dimensional and non-dimensional format to aid in interpretation. These results build upon earlier parametric and blade cost studies, which were used as a guide for the innovative design approaches explored here.

Acknowledgements

TPI Staff: Derek Berry and Steve Lockard
Dynamic Design: Kevin Jackson
MDZ Consulting: Mike Zuteck
University of California, Davis: Case Van Dam

Sandia Technical Monitors: Tom Ashwill
Paul Veers

This is a Contractor Report for Sandia National Laboratories that partially fulfills the deliverables under Contract #15890.

TABLE OF CONTENTS

LIST OF FIGURES

LIST OF TABLES

1.0 ANALYSIS APPROACH

1.1 Goals and Objectives

The primary goal of the WindPACT Blade System Design Study (BSDS) was investigation and evaluation of design and manufacturing issues for wind turbine blades in the one to ten megawatt size range. The results of the initial engineering study [1] will guide design specifications and preliminary engineering for candidate blades in the range of 30 to 70 meters in length. Subsequent efforts will generate detailed recommendations for sub-scale and sub-structure testing that will help determine the feasibility of innovations and provide data for detailed design in follow-on contracts.

The initial project task was to assess the fundamental physical and manufacturing issues that govern and constrain large blades. The issues and constraints phase of the project entails three basic elements: 1) a parametric scaling study to assess blade structure using current technology [1], 2) an economic study of the cost to manufacture, transport, and install large blades [2], and 3) identification of promising innovative design approaches that show potential for overcoming fundamental physical and manufacturing constraints (documented in this report).

This report discusses several innovative design approaches and their potential for blade cost reduction. During this effort we reviewed methods for optimizing the blade cross-section to improve structural and manufacturing characteristics. We also analyzed and compared a number of composite materials and evaluated their relative merits for use in large wind turbine blades in the range from 30 meters to 70 meters. The results have been summarized in dimensional and non-dimensional format to aid in interpretation. These results build upon earlier parametric and blade cost studies [1,2], which were used as a guide for the innovative design approaches explored here.

1.2 Summary of Parametric Study Results

The large blade parametric review [1] estimated peak power output, annual energy capture, design bending moments, blade laminate weight, and tip deflection for megawatt scale wind turbines with rotors of 62, 83, 104, 125, and 146 meters in diameter. The annual energy production for each rotor size was evaluated as a function of tip speed at 60, 65, and 70 m/s, which brackets the operating range of typical commercial wind turbines.

The NREL S821 was selected as the baseline airfoil used in the aerodynamic scaling study. A series of scaled airfoil versions were developed and analyzed. The maximum thickness-to-chord ratio (t/c) was modified in increments of approximately 5%, starting at 24% for the S821 and ending with an extreme design case of 60% t/c.

Blade design loads were estimated using two simplified methods: parked under extreme winds and an operating gust condition. The first model calculated the extreme loads with the turbine in the parked condition in accordance with IEC Class I design recommendations. The second calculation method estimated blade spanwise loading under high wind gust conditions. Both load estimation approaches provided similar results with regards to the blade design loads.

Structural analyses of three representative blades ("baseline", "thicker", and "thickest") were performed at representative spanwise stations. The blade construction was assumed to be a stressed shell, which was composed of four primary components: a low pressure shell on the downwind side, a high pressure shell on the upwind side, and two shear webs bonded between the two shells. The properties of the blade cross-sections were computed at several stations, which were used to estimate stress and deflection using standard two-dimensional beam theory.

In the blade range from 30 to 70 meters the blade weight grew as the cube of the length for all three cross-sections studied. The economic performance of the blades is inversely related to the specific weight, defined as the blade weight divided by capture area (kg/m^2), which more than doubled over the same range.

Increased airfoil section thickness appears to be a key tool in limiting blade weight and cost growth with scale. Thickened and truncated trailing edges in the inboard region provide strong, positive effects on blade structural performance. From the thin to thickest blade distribution the specific weight was reduced by 15%, due to increased structural performance.

1.3 Summary of Cost Study Results

The cost study [2] reviewed critical fabrication and transportation constraints as a function of blade length. The cost of large wind turbine blades was estimated using an analytical model that was applied to each of the three blade sizes (30 m, 50 m and 70 m). The cost estimation approach assumed that currently available technology would be used and included materials, labor, development, facilities, and transportation costs. Laminate requirements obtained from the structural model were used to develop a bill of materials and manufacturing task list. Blade development costs included engineering design and documentation, fabrication of tooling and prototypes, and the cost of static, fatigue, and operational field testing.

Facilities costs were calculated based upon the size of the rotor blades using manufacturing plant layouts developed specifically for each size. Each of the three potential manufacturing facilities was sized to provide a constant annual rated power production (approximately 650 to 700 MW per year).

The costs of transportation were developed assuming overland trucking. The cost study considered several different manufacturing plant locations in the Northeast, Southwest, and Western United States and estimated the cost for trucking the blades to a number of wind sites. The study also identified potential constraints for movement of large blades on public roadways.

The results of the large blade cost study indicate that blade materials become a greater proportion of total blade cost, while the percentage of labor cost is decreased as blade size grows. Blade development costs were found to increase substantially with scale as a result of the higher prototype costs and the shorter production runs over which to amortize development costs. Transportation costs decreased as a percentage of total cost because total blade cost increased; however, size and weight limits were found to constrain shipment of blades larger than 50 meters and strongly influence transport costs of blades above that length.

The results of the large blade cost study indicate that overall blade cost scales at a rate less than the growth in the weight. This was due primarily to a lower rate of growth for estimated manufacturing labor costs. Many of the cost categories were found to be proportional to blade area, rather than material volume. Even with a somewhat more favorable scaling trend, the blade cost share as a percentage of the total turbine installed cost can be expected to nearly double when the blade size increases from 30 to 70 meters. The large blade cost study also suggested that blade cost reduction efforts should focus on reducing material cost and lowering manufacturing labor requirements. Cost reductions in those areas were found to have the strongest impact on overall blade cost.

1.4 Blade Planform Definition

The innovative approaches evaluation assumed a reference blade length of 50 meters. The blade planform characteristics were as shown in Table 1.1 and Figure 1.1. The wind turbine was assumed to have a conventional, three bladed rotor with the blades mounted at the root to a central hub.

Table 1.1 Blade Planform Summary

Radius Ratio	Radius (m)	Chord Ratio	Chord (m)	Twist (deg)
5%	2.600	5.2%	2.690	29.5
15%	7.800	7.8%	4.030	19.5
25%	13.000	8.6%	4.472	13.0
35%	18.200	7.6%	3.939	8.8
45%	23.400	6.6%	3.452	6.2
55%	28.600	5.7%	2.986	4.4
65%	33.800	4.9%	2.534	3.1
75%	39.000	4.0%	2.092	1.9
85%	44.200	3.2%	1.659	0.8
95%	49.400	2.4%	1.233	0.0

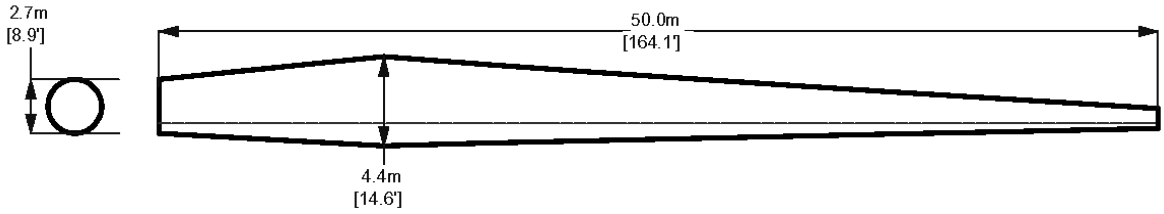

Figure 1.1 Blade Planform Drawing

1.5 Blade Design Loads

Blade extreme wind design loads were estimated in accordance with IEC Class I recommendations and are provided in Table 1.2. The analysis method assumed the wind speed was 70 m/s at the rotor hub and wind shear increased with hub height according to a power law. Standard air density and an IEC recommended partial load factor of 1.35 were assumed in the analysis. Blade aerodynamic forces were generated using the flat plate drag coefficient for the proper Reynolds number.

Table 1.2 Blade Extreme Wind Design Bending Moments

Rotor Station (%)	Bending Moment (kNm)	Rotor Station (%)	Bending Moment (kNm)
0.0%	20198	50.0%	3640
10.0%	15763	60.0%	2118
20.0%	11738	70.0%	1067
30.0%	8380	80.0%	415
40.0%	5704	90.0%	90

1.6 Blade Structural Design

Structural analyses of three blade sizes were performed at representative spanwise stations. The properties of the blade cross-sections were computed using standard two-dimensional beam theory. The blade construction was assumed to be a stressed shell, which was composed of four primary components: a low pressure (LP) shell on the downwind side, a high pressure (HP) shell on the upwind side, and two shear webs bonded between the two shells as shown in Figure 1.2.

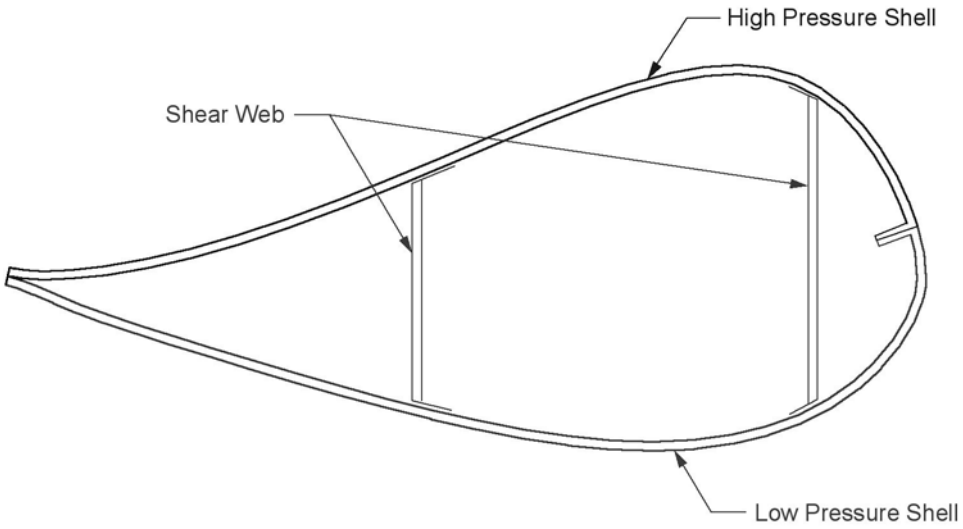

Figure 1.2 Schematic of Blade Construction

2.0 STRUCTURALLY OPTIMIZED BLADE CROSS-SECTIONS

2.1 Evaluation of Section Characteristics

The innovative sub-system design task was organized such that blade structural manufacturing design issues were used to initiate the blade development process. The baseline blade planform and thickness distribution were modified in the inboard blade region to optimize structural material placement and blade strength. The resulting structurally optimized thickness distribution is presented and discussed in the following chapter (Chapter 3 – Structurally Optimized Blade Thickness). However, during this effort it became apparent that the cross-sectional shape of the S821and its derivatives were poor in terms of structural efficiency. This is because chordwise position of maximum thickness for the upper surface does not correspond with the maximum thickness position of the lower surface. Realization of this problem led to an evaluation of the structural effectiveness of other potential inboard cross-sectional shapes.

A total of six different blade section shapes were compared based on their aerodynamic properties and structural characteristics: DU97-W-300, S821-30, FFA-W3-301, LS(1)-0421Mod-30, NACA63-430, Hybrid-30.0-1.7. These various section shapes are plotted graphically in Figure 2.1 for comparison purposes. The first plot exaggerates the vertical scale to provide a better comparison between airfoils, while the second plot shows all the airfoils in true scale.

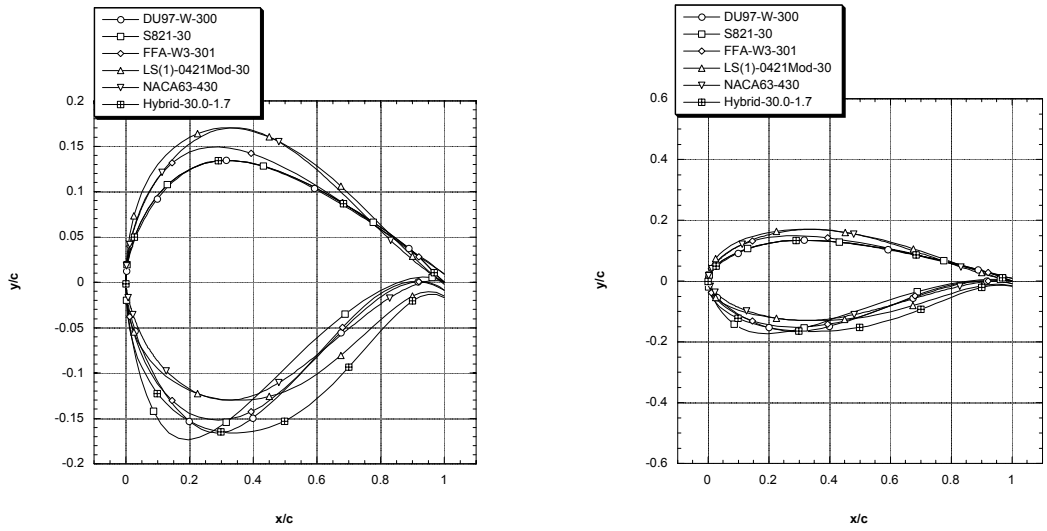

Figure 2.1 Comparison of Root Section Shapes (t/c = 0.30)

The wind energy group at Delft University of Technology designed the DU97-W-300 airfoil [3]. This airfoil was specifically designed for wind turbine blades. It has a blunt trailing edge ($t_{te}/c = 0.0174$) and a maximum thickness-to-chord ratio (t/c) of 0.30.

The S821-30 was developed earlier during this effort by scaling-up the thickness distribution of the S821 [4] from its t/c = 0.24 to t/c = 0.30 while leaving the camber distribution unchanged. This airfoil has a sharp trailing edge.

The FFA-W3-301 is one of the most popular root section shapes [5]. It has a t/c = 0.30 and a blunt trailing edge (t_{te}/c = 0.0183).

The LS(1)-0421Mod-30 is a scaled-up version of the LS(1)-0421Mod airfoil [6]. Its camber distribution is unchanged but the new airfoil has a t/c=0.30. Also it has a blunt trailing edge with a t_{te}/c = 0.0129 (unchanged from the baseline airfoil).

The NACA63-430 airfoil has a t/c = 0.30 and a sharp trailing edge [7].

The Hybrid-30.0-1.7 is a proof-of-concept airfoil combining the upper surface of the S821-30 and a scaled-up lower surface of the LS(1)-0421Mod. The resulting sectional shape is a first attempt in the structurally driven design process. It was not purposefully designed for aerodynamic performance and could likely be improved with additional effort. The Hybrid section has a t/c = 0.30 and a t_{te}/c = 0.0167. The goal was to achieve a more efficient structural shape than the S821 and DU97-W-300 without losing too much of the desirable reduced aerodynamic sensitivity to surface roughness of the NREL S-type and Delft DU-type airfoils. Figure 2.2 compares the S821-30, LS(1)-0421Mod-30, and the Hybrid airfoil.

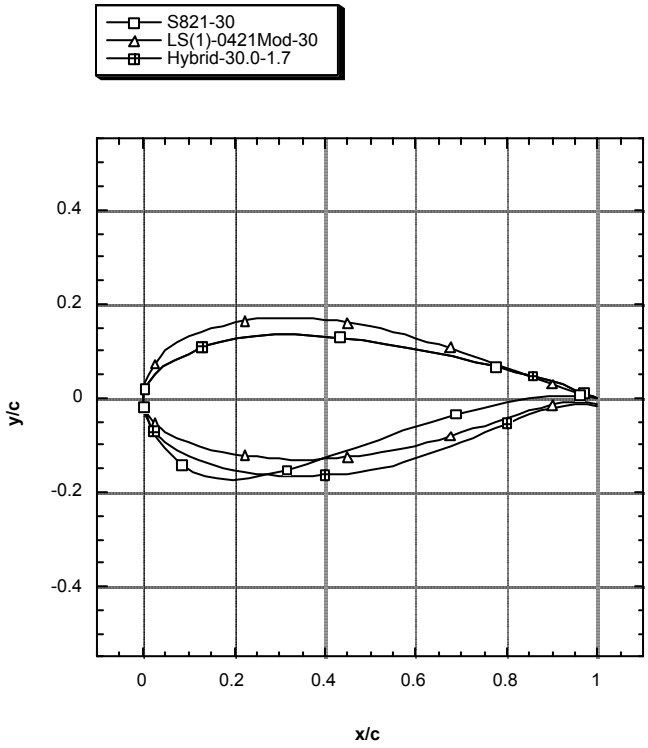

Figure 2.2 Comparison of Base and Hybrid Section Shapes

Table 2.1 presents an overview of the structural and aerodynamic characteristics of these airfoils. The parameter h is the overall height of the airfoil and is equal to the maximum surface height minus the minimum surface height over the full chord of the section. For all airfoils, except the S821-30, h is nearly identical to t, which is the section height at a particular chordwise location. The structural quantities presented in Table 2.1 are the non-dimensional sectional or profile area, $\int ydx/(hc)$, and the non-dimensional sectional moment of inertia, $\int y^2dx/(ch^2/2)$. The former provides a measure of blade volume whereas the latter provides a measure of the bending stiffness of a thin-skin structure.

Table 2.1 Comparison of Several Alternative Blade Section Characteristics

Cross-Section Designation	DU97-W-300	S821-30	FFA-W3-301	LS(1)-0421Mod-30	NACA63-430	Hybrid-30-1.7
t/c	.30	.30	.30	.30	.30	.30
h/c	.300	.307	.301	.300	.300	.300
$\int ydx/(hc)$	.587	.566	.605	.659	.602	.665
$\int y^2dx/(ch^2/2)$	.453	.438	.475	.542	.486	.541
$c_{l_{max}}$ @ Re = 2.3×10^6 (free)	1.725	1.784*	2.003*	1.619*	1.704	1.653*
$\alpha_{cl_{max}}$ (deg)	13.5	16.0*	16.0*	16.0*	13.0	16.0*
$c_{l_{max}}$ @ Re = 2.3×10^6 (fixed)	1.481	1.470	1.431	1.272*	1.145*	1.317*
$\alpha_{cl_{max}}$ (deg)	14.0	15.5	12.25	16.0*	16.0*	16.0*
$\Delta c_{l_{max}}$ due to roughness	0.244	0.314	0.572	0.347	0.559	0.336
$(c_l/c_d)_{max}$ @ Re = 2.3×10^6 (free)	120.9	110.7	117.3	109.2	136.0	103.1
$c_{l_{(L/D)max}}$	1.562	1.332	1.601	1.198	1.418	1.204
$(c_l/c_d)_{max}$ @ Re = 2.3×10^6 (fixed)	66.8	62.2	64.2	37.3	35.7	50.7
$c_{l_{(L/D)max}}$	1.285	1.171	1.273	0.752	0.641	1.038
$\Delta(c_l/c_d)_{max}$ due to roughness	54.1	48.5	53.1	71.9	100.3	52.4
$c_{d_{min}}$ @ Re = 2.3×10^6	0.00941	0.00952	0.00923	0.00740	0.00761	0.00795
(counts)	94.1	95.2	92.3	74.0	76.1	79.5

The aerodynamic characteristics are predicted using the viscous-inviscid interaction method MSES[8]. We have some concerns regarding the accuracy of this type of methodology for these thick airfoils. However, all airfoils are analyzed in an identical manner and as such the results presented here provide a reasonable way to compare the section characteristics. Future efforts should focus on validating these results using more complete methods (Reynolds-averaged Navier Stokes) and/or wind tunnel testing. In Table 2.1 the most important aerodynamic performance results are summarized. The detailed results are presented in Figures 2.3 and 2.4. For purposes of this analysis the free transition case corresponds to clean blade surfaces, while the fixed transition case would represent soiled or contaminated surfaces. The fixed transition was specified near the leading edge at x/c = 0.02 on the upper surface and x/c = 0.05 on the lower surface.

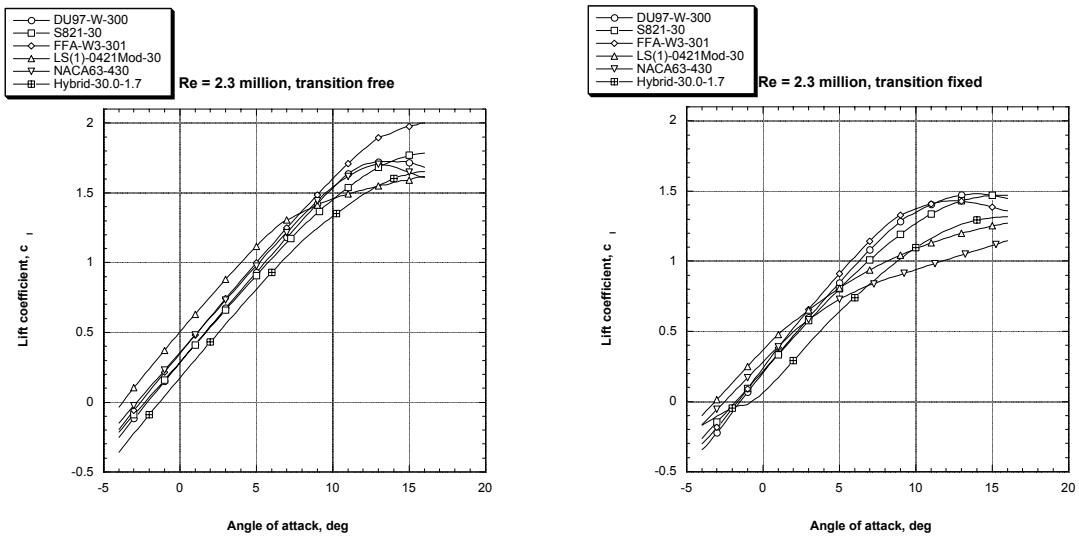

Figure 2.3 Comparison of Lift Curves (Free and Fixed Transition)

The results show the Hybrid-30.0-1.7 to be structurally most efficient whereas the DU97-W-300 airfoil is aerodynamically most efficient with transition fixed. Figures 2.5 to 2.8 present the tradeoffs between structural efficiency and aerodynamic performance. These plots show that the Hybrid airfoil provides a reasonable compromise in aerodynamic and structural characteristics for use in large rotor blades.

Note that we do not claim this section shape to be optimal and undoubtedly its aerodynamic performance characteristics can be improved without too much loss in structural efficiency. The Hybrid used here was believed to be a reasonable candidate that could be used to assess the potential for more optimal sections in this study.

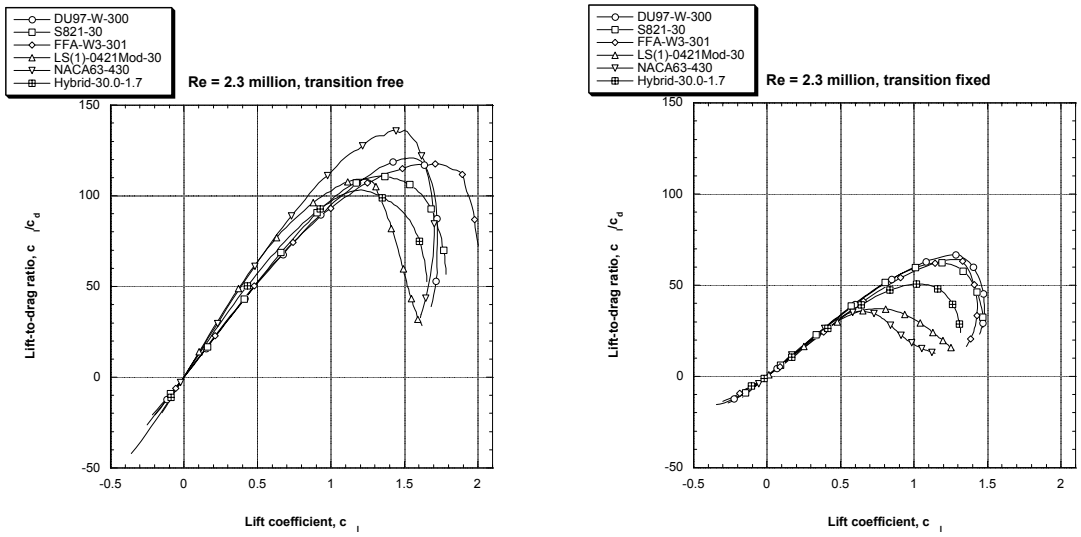

Figure 2.4 Comparison of Lift-to-Drag Curves (Free and Fixed Transition)

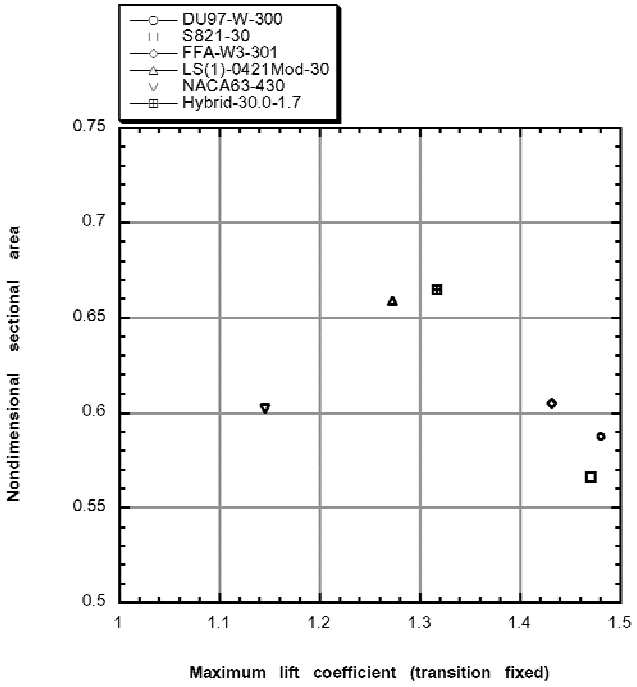

Figure 2.5 Diagram Comparing Structural (Sectional Area) and Aerodynamic Characteristics (Maximum Lift Coefficient)

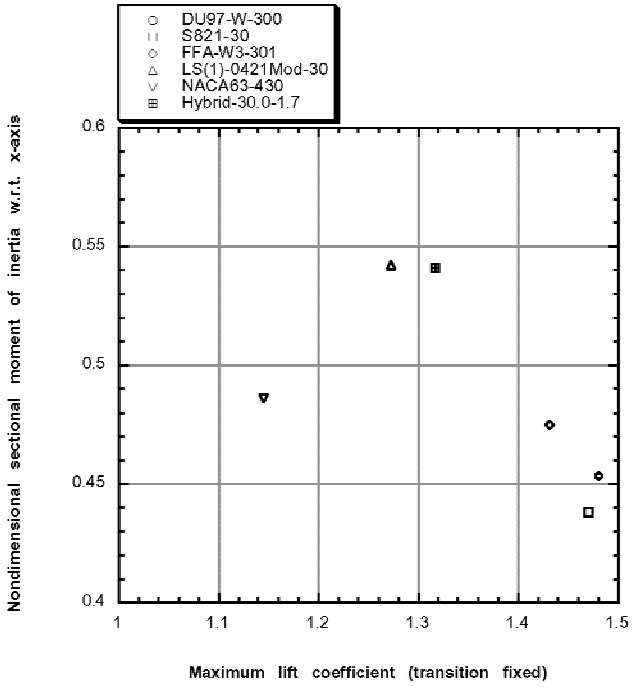

Figure 2.6 Diagram Comparing Structural (Sectional Moment of Inertia) and Aerodynamic Characteristics (Maximum Lift Coefficient)

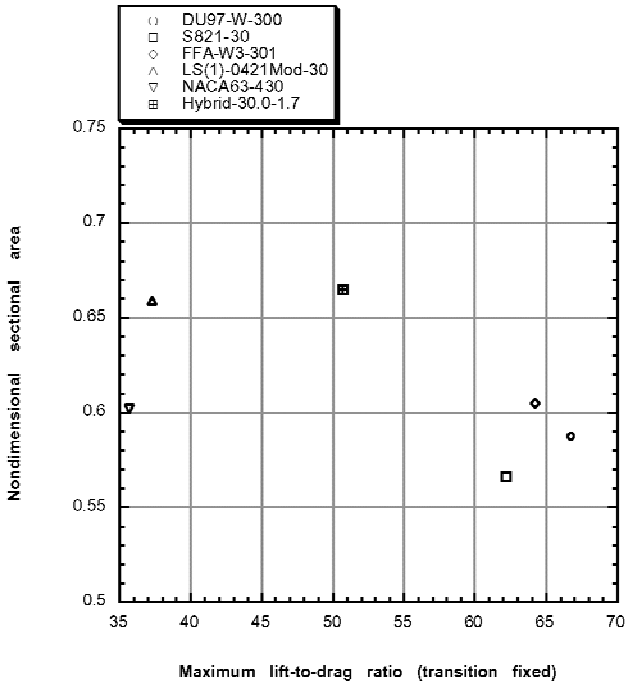

Figure 2.7 Diagram Comparing Structural (Sectional Area) and Aerodynamic Characteristics (Maximum Lift-to-Drag Ratio)

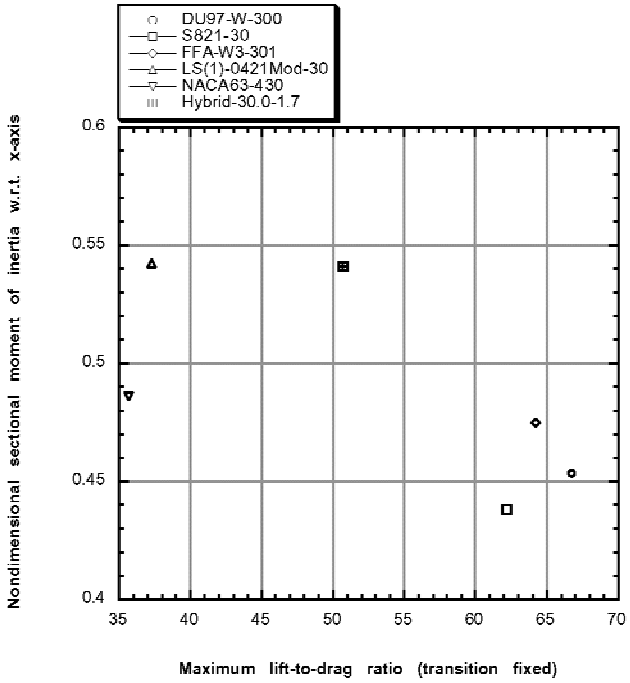

Figure 2.8 Diagram Comparing Structural (Sectional Moment of Inertia) and Aerodynamic Characteristics (Maximum Lift-to-Drag Ratio)

2.2 Selection of a Candidate Hybrid Section

During our review of the section properties we determined that a hybrid section shape would best meet the project structural and manufacturing design goals. This shape was pieced together using the upper surface shape of the S821-30 and the lower surface shape of the LS(1)-0421Mod-30 (Figures 2.2 and 2.9) and has an overall thickness ratio of 27%. The shape of the hybrid has much improved structural characteristics, while preserving reasonable aerodynamic performance. There was no attempt made to design a fully optimized airfoil, rather the hybrid was generated to quickly identify and evaluate the importance of section shape on blade structural efficiency, material weight, and manufacturing cost.

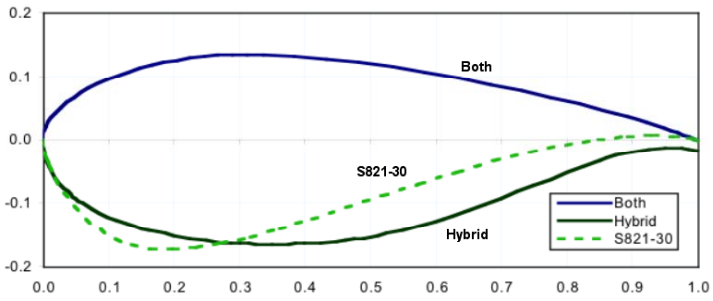

Figure 2.9 Comparison of S821-30 and Hybrid Airfoil Sections

3.0 STRUCTURALLY OPTIMIZED BLADE THICKNESS

3.1 Constant Spar Cap Concept

The basic concept for creating the structurally optimized blade was to provide a constant thickness spar cap for most of the inboard blade. We used the selected candidate hybrid section at station 55% r/R to size the spar cap, and then increased the section thickness ratio (t/c) to meet the increasing flapwise design bending moment going inward, without changing the spar cap width or thickness. This approach to simplifying and improving the blade design had been suggested by the slow change of spar cap area in the initial studies of the thickest of the parametric blade variations.

The constant spar cap concept offers both structural and manufacturing benefits. In particular, the elimination of laminate ply drops along the length will increase spar cap fatigue strength. The negative effect of ply drops has been documented in the literature [9] and has a negative effect on the fatigue life curve. For this study we did not directly account for the benefits of fatigue strength improvement in our calculations and further weight savings can be expected beyond those estimated here.

In addition to improved fatigue lifetime, the long run of constant spar cap reduces the need to cut materials to width, thereby reducing scrap material and labor. Simplification of the spar cap lay-up could also be expected to save some labor in the kitting and material placement operations. Again the benefits to manufacturing were not directly calculated in this phase of work, but they are believed to be real and economically significant.

3.2 Structural Optimization Methodology

The initial blade thickness distribution was derived from the earlier parametric study[1]. In this effort we defined a baseline distribution, a high thickness/sharp trailing edge distribution, and a distribution that based upon the structurally improved hybrid airfoil. Thickness of the hybrid airfoil was increased as necessary at inboard stations by truncating the trailing edge sections shown in Figure 3.1. The nomenclature for the airfoil series is Hybrid-tt-zz, where tt is the airfoil thickness and zz is the trailing edge thickness as a percentage of chord.

This phase of the effort defined a new thickness distribution, structurally optimized by applying the constant spar cap concept (Table 3.1). The candidate hybrid section was chosen as the primary airfoil for station 55 (55% r/R). This blade station used a 27% thick hybrid section described in Section 2.2. The thickness ratio was then calculated at stations 45, 35, 25, and 15 using the design bending moment and the fixed spar cap geometry.

Table 3.1 Blade Planform and Thickness Distributions

Station Number	Baseline Thickness Ratio	Baseline Thickness (mm)	Thick Sharp Thickness Ratio	Thick Sharp Thickness (mm)	Hybrid Truncated Thickness Ratio	Hybrid Truncated Thickness (mm)
5	100.00%	2690	100.00%	2690	100.00%	2690
15	42.00%	1693	62.00%	2499	63.00%	2539
25	28.00%	1252	48.00%	2147	48.50%	2169
35	24.00%	945	40.00%	1576	41.20%	1623
45	23.00%	794	33.00%	1139	33.60%	1160
55	22.00%	657	26.00%	776	27.00%	806
65	21.00%	532	21.00%	532	21.00%	532
75	20.00%	418	20.00%	418	20.00%	418
85	19.00%	315	19.00%	315	19.00%	315
95	18.00%	222	18.00%	222	18.00%	222

Initially the hybrid section was scaled to 30% t/c by geometric (x-y) scaling. To generate higher thickness ratios the section was progressively truncated by removing chord from the trailing edge. This formed sections with large flat trailing edges that provided improved structural efficiency. A 35% t/c base truncated airfoil was geometrically scaled to provide the station 45 airfoil, while a 40% t/c base was used at station 35, and a 45% t/c base was used at stations 25 and 15.

An analysis of the structural properties was performed at each station. The required section thickness was determined by iteration until the required flapwise moment capability was obtained assuming IEC Class 1 extreme wind loads. A trailing edge spline, consisting of unidirectional fiber located near the trailing edge, was incorporated into the flat trailing edge panel. The size of the trailing edge spline was adjusted as required to meet the edgewise bending moment requirement.

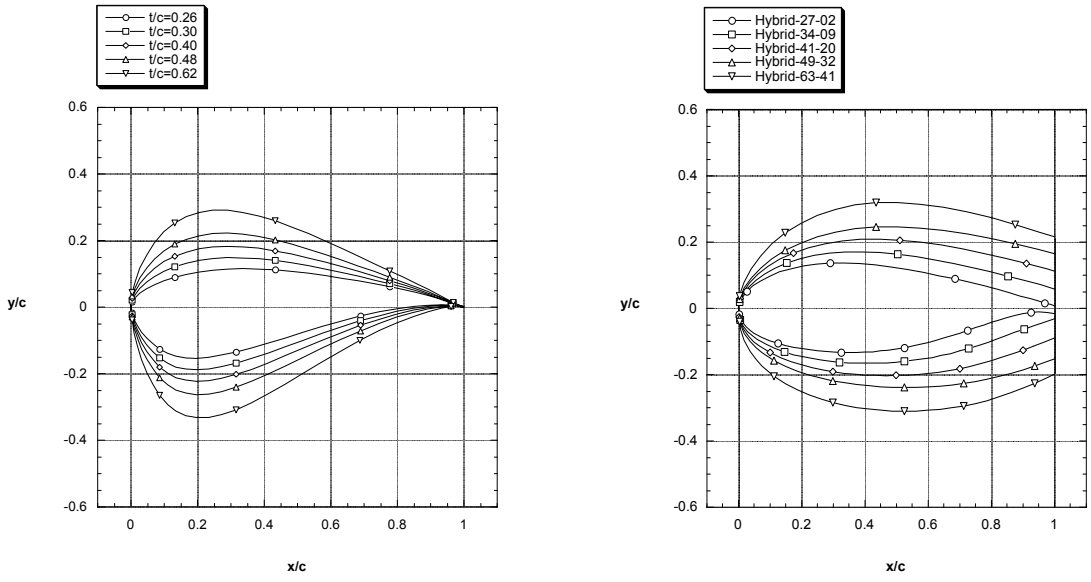

Figure 3.1 Comparison of Thick-Sharp and Hybrid Truncated Sections

The final structurally optimized (hybrid-truncated) thickness distribution was nearly identical to the thickest (thick-sharp) distribution evaluated in the parametric study (Figures 3.2 and 3.3), although that was not due to conscious efforts to make the two distributions match. The close match between the two distributions was coincidental and an unexpected result. If the blade was optimized for a different design load distribution the results would change. For example, optimizing the blade for an IEC Class II wind site (instead of Class I) would reduce design bending moment requirements and section thickness for the inboard stations.

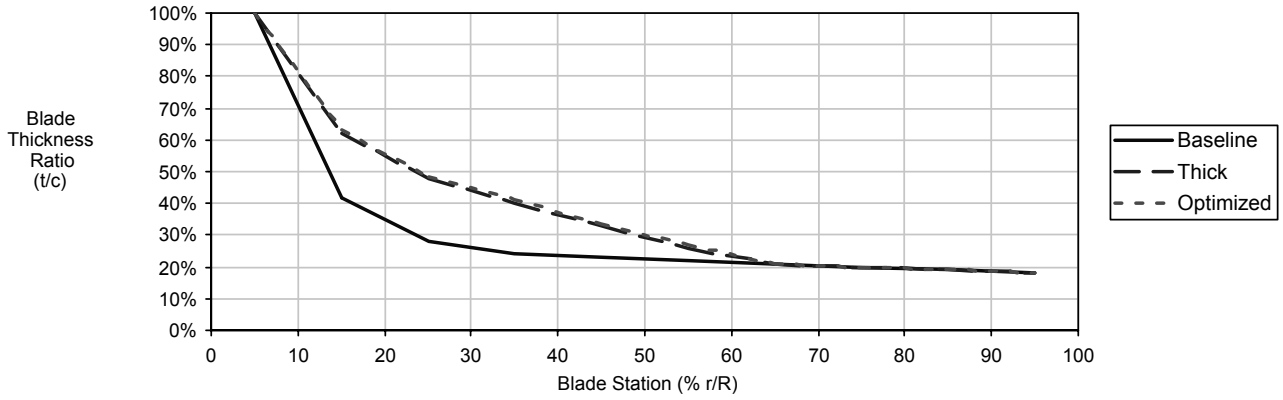

Figure 3.2 Comparison of Non-Dimensional Blade Thickness Distributions

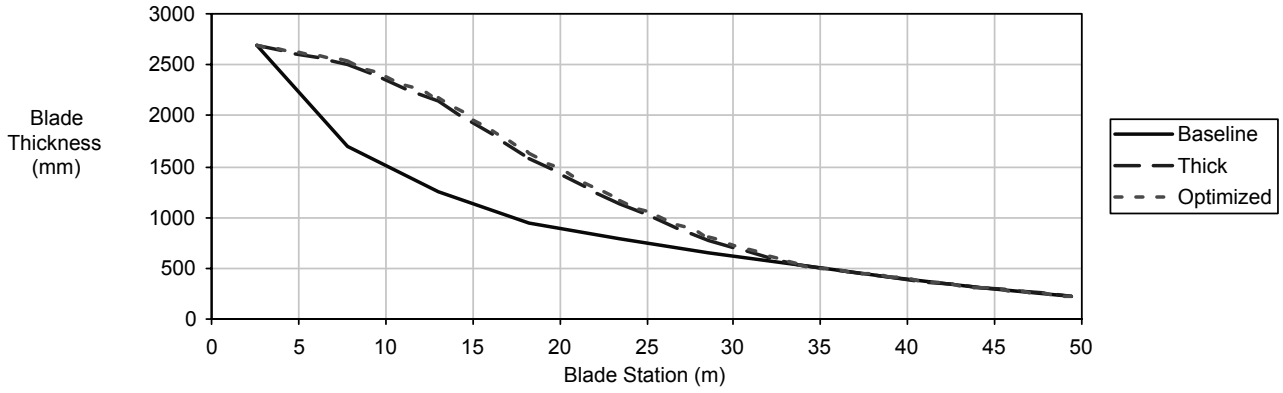

Figure 3.3 Comparison of Dimensional Blade Thickness Distributions

3.3 Results

The blade weight, spar cap weight, and spar cap material cost were calculated for E-glass material, using the same material properties and costs as were used in the cost comparison study [2]. The 50m baseline blade with truncated hybrid sections was found to have a blade shell weight of 9872 kg (21,718 lbs), some 213 kg (469 lbs) less than the thick-sharp E-glass design. The reduction of spar cap weight was 401 kg (882 lbs), but some of that was offset by materials needed to create the flat trailing edge panel. The computed spar cap cost was $20,704, $1,676 (about 7%) less than the $22,380 estimated for the thick-sharp blade. Some of that savings would be given back to the aft panel. It should be emphasized that this exercise was only a first look at the possible effect of

truncation. More rigorous tradeoff of degree of truncation versus weight and cost should give better results. The primary purpose of this analysis was to provide an initial indication of the level of improvement that might be possible and to thereby provide a basis to decide if further work is warranted.

3.4 Further Evolution

In performing the structural calculations, it was found that the aft panel trailing edge spline was only a few millimeters thick, and fairly constant in thickness. If the trailing edge flat was made smaller, the spline thickness could be increased so the aft panel balsa core assumed in the section analysis wouldn't be necessary. This would save some cost, and a narrower trailing edge might also benefit power production. By choosing a suitable width profile, the trailing edge spline thickness could be held constant. This would seem to be a nearly ideal application for zebrawood, which has both high stiffness-to-weight, excellent fatigue characteristics, and good damping properties. Zebrawood (described in Section 5.5) offers a simple, low cost option in this flat panel application.

4.0 PERFORMANCE IMPLICATIONS OF BLADE CROSS-SECTIONS

4.1 Performance of Baseline Sections

The lift and drag properties of the baseline S821-xx cross-sections were computed using MSES [8] for both free and fixed transition cases. Performance in the free transition case will be representative of clean blades, while the fixed transition case approximates the results expected from blades that are soiled and have significant leading edge roughness.

Turbine power curves and annual energy estimates were developed using a performance model. The rotor aerodynamic performance was calculated using blade element momentum theory (PROP code). The turbine was assumed to have a rotor diameter of 102 meters, a rated power of 3 MW, and active power regulation. It was further assumed that the turbine operated with a fixed tip speed of 70 m/s. Standard air density was assumed (1.225 kg/m^3) and wind speed was assumed to be constant across the rotor disc. Annual energy calculations assumed a Rayleigh wind speed distribution and 100% availability. Drivetrain performance losses were modeled assuming the gearbox and generator efficiencies provided in Tables 4.1 and 4.2.

Table 4.1 Assumed Gearbox Efficiency

Load (MW)	Gearbox Efficiency
0.0	1.0%
0.1	70.0%
0.2	80.0%
0.5	89.0%
0.9	94.0%
1.4	96.0%
1.8	97.0%
2.3	98.0%
3.0	98.0%

Table 4.2 Assumed Generator Efficiency

Load (MW)	Generator Efficiency
0.0	1.0%
0.3	83.5%
0.7	90.0%
1.4	91.5%
2.1	91.5%
2.8	91.0%
3.0	91.0%

Power curves for the baseline rotor thickness distribution and NREL type airfoils were calculated first and are shown in Figure 4.1. The calculations included both free and fixed transition, representing clean and soiled conditions respectively. Energy capture for several pitch angles and average wind speeds are summarized in Table 4.3, assuming a Rayleigh wind distribution and 100% turbine availability.

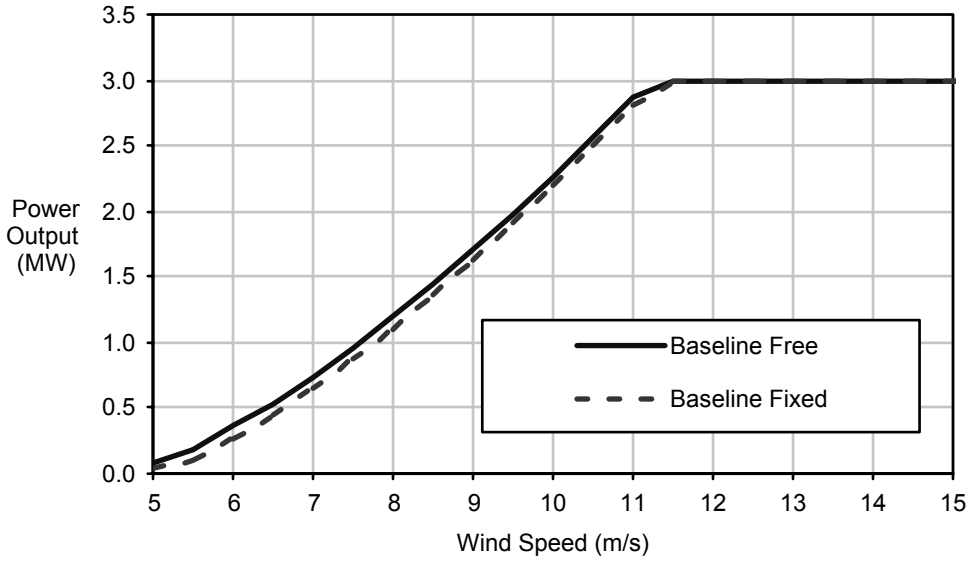

Figure 4.1 Baseline Performance Comparison for Free and Fixed Transition

Table 4.3 Baseline Energy Capture for Several Pitch Settings

Wind Speed (m/s)	-2° Pitch		-1° Pitch		0° Pitch	
	Free (MWh)	Fixed (MWh)	Free (MWh)	Fixed (MWh)	Free (MWh)	Fixed (MWh)
5.5	4876	4579	5023	4666	5103	4682
6.0	6176	5865	6320	5944	6391	5944
6.5	7477	7160	7615	7231	7676	7215
7.0	8736	8420	8866	8481	8917	8453

4.2 Performance of Thick Sections With Sharp Trailing Edges

The next analysis evaluated the performance of a rotor using thick sections, which had sharp trailing edges and were not truncated. Sections were scaled from the baseline S821 airfoil to match the thick-sharp distribution summarized in Table 3.1. Lift and drag characteristics were calculated for the sections using MSES for both free (clean) and fixed (soiled) transition and are thus directly comparable to the baseline aerodynamic properties.

A comparison between the power curves for the baseline and the thick-sharp sections is provided in Figures 4.2 and 4.3. These plots show that there is relatively little performance loss for the thick distribution when the blades are clean (free transition), but rather large losses in performance when the blades are soiled (fixed transition). Annual energy capture for the thick-sharp sections is summarized in Table 4.4. An energy capture comparison between the baseline and the thick-sharp rotor is provided in Table 4.5. Losses for the thick section blades ranged between 1.2% to 2.2% for clean blades (free transition) and 4.7% to 7.0% for soiled (fixed transition) conditions.

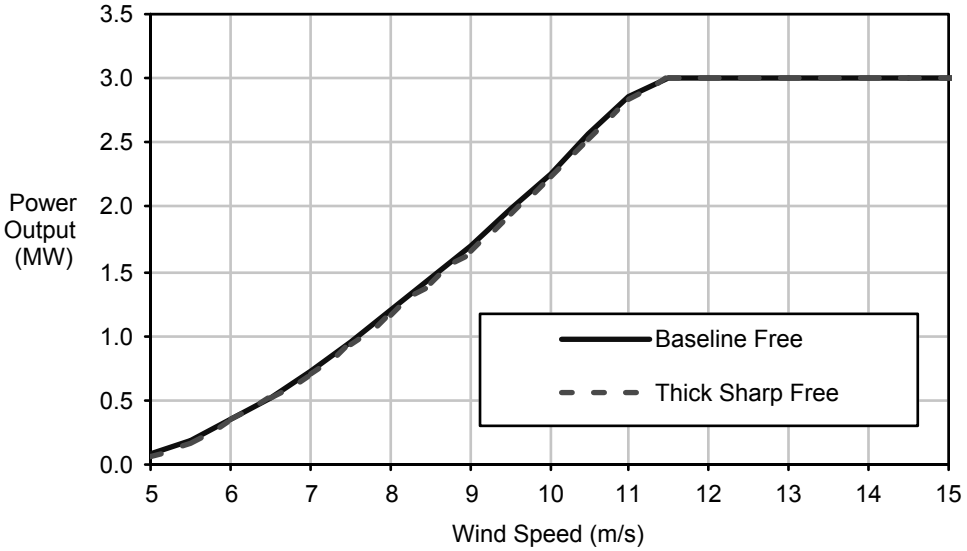

Figure 4.2 Comparison Between Thick-Sharp and Baseline Performance Assuming Free Transition

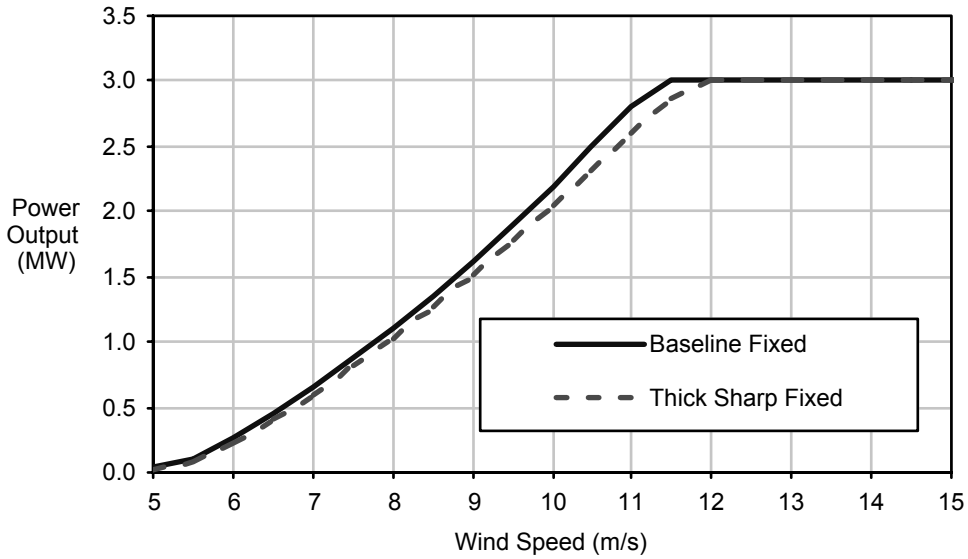

Figure 4.3 Comparison Between Thick-Sharp and Baseline Performance Assuming Fixed Transition

Table 4.4 Thick-Sharp Section Energy Capture for Several Pitch Settings

Wind Speed (m/s)	-2° Pitch		-1° Pitch		0° Pitch	
	Free (MWh)	Fixed (MWh)	Free (MWh)	Fixed (MWh)	Free (MWh)	Fixed (MWh)
5.5	4790	4296	4928	4367	4989	4353
6.0	6080	5533	6215	5599	6267	5566
6.5	7375	6790	7503	6850	7545	6800
7.0	8631	8022	8751	8075	8783	8012

Table 4.5 Thick-Sharp Energy Capture Comparison to Baseline

Wind Speed (m/s)	-2° Pitch		-1° Pitch		0° Pitch	
	Free (MWh)	Fixed (MWh)	Free (MWh)	Fixed (MWh)	Free (MWh)	Fixed (MWh)
5.5	-1.77%	-6.19%	-1.90%	-6.41%	-2.24%	-7.03%
6.0	-1.55%	-5.66%	-1.66%	-5.81%	-1.95%	-6.35%
6.5	-1.36%	-5.17%	-1.47%	-5.27%	-1.71%	-5.74%
7.0	-1.21%	-4.72%	-1.30%	-4.79%	-1.51%	-5.21%

4.3 Performance of Hybrid Truncated Sections

The final analysis estimated rotor performance using hybrid sections that had been truncated at the trailing edge as shown in Figure 3.2. Lift and drag characteristics were calculated using MSES for both free and fixed transition, as was done for both the baseline and thick-sharp sections.

A comparison between the power curves for the baseline, thick-sharp, and hybrid truncated sections is provided in Figures 4.4 and 4.5. These plots show that there is relatively little performance difference between the three distributions when the blades are clean (free transition). The hybrid truncated blades also minimized losses in performance when the blades are soiled (fixed transition) as compared against the thick-sharp sections. Annual energy capture for the hybrid truncated sections is summarized in Table 4.6. An energy capture comparison between the hybrid truncated and the baseline rotor is provided in Table 4.7. Losses for the thick section blades ranged between 1.5% to 2.8% for clean blades (free transition) and 2.5% to 3.7% for soiled (fixed transition) conditions.

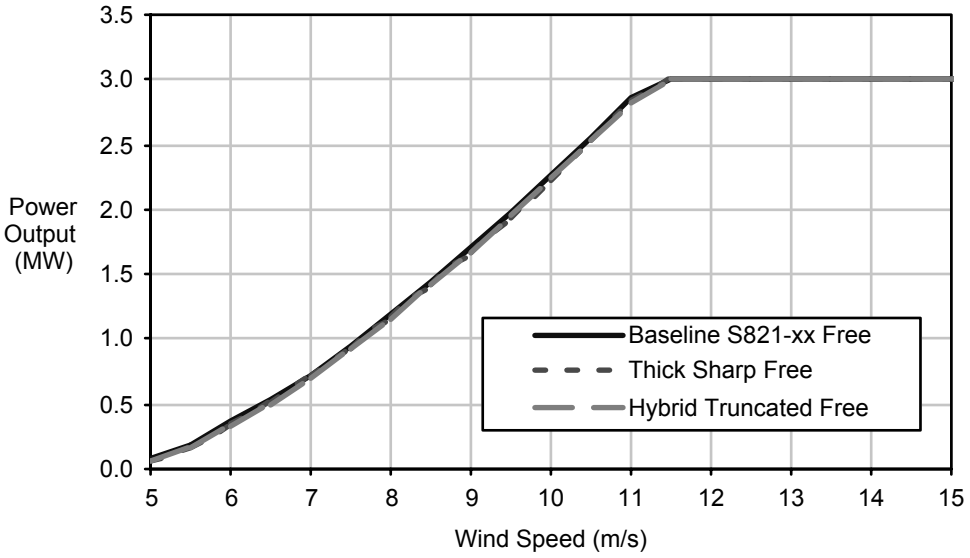

Figure 4.4 Comparison Between Hybrid Truncated, Thick-Sharp ,and Baseline Performance Assuming Free Transition

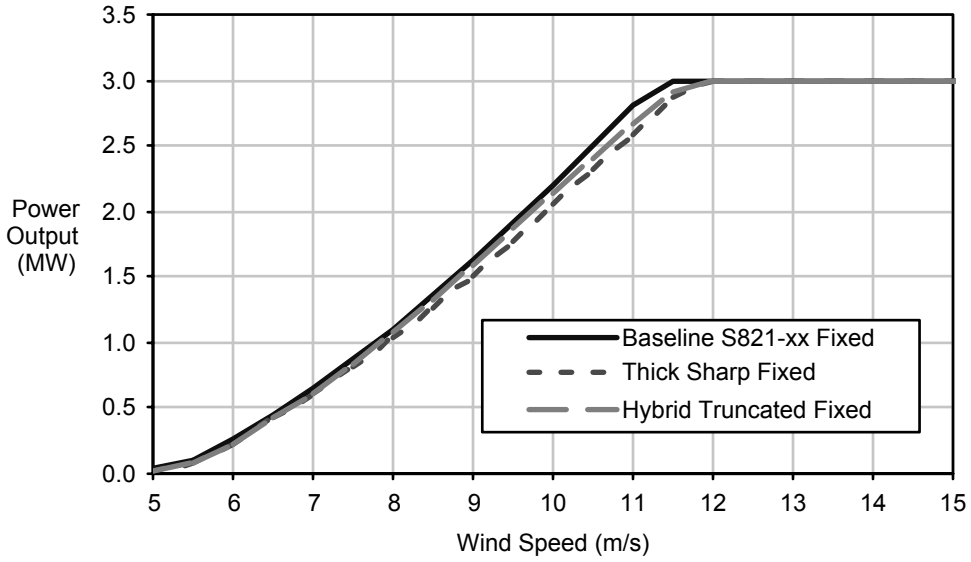

Figure 4.5 Comparison Between Hybrid Truncated, Thick-Sharp ,and Baseline Performance Assuming Fixed Transition

Table 4.6 Hybrid Truncated Section Energy Capture for Several Pitch Settings

Wind Speed (m/s)	-2° Pitch		-1° Pitch		0° Pitch	
	Free (MWh)	Fixed (MWh)	Free (MWh)	Fixed (MWh)	Free (MWh)	Fixed (MWh)
5.5	4764	4415	4898	4502	4960	4508
6.0	6054	5671	6187	5759	6242	5751
6.5	7350	6942	7477	7029	7524	7008
7.0	8606	8183	8727	8268	8766	8236

Table 4.7 Hybrid Truncated Energy Capture Comparison to Baseline Section

Wind Speed (m/s)	-2° Pitch		-1° Pitch		0° Pitch	
	Free (MWh)	Fixed (MWh)	Free (MWh)	Fixed (MWh)	Free (MWh)	Fixed (MWh)
5.5	-2.30%	-3.59%	-2.48%	-3.53%	-2.81%	-3.71%
6.0	-1.96%	-3.31%	-2.10%	-3.12%	-2.34%	-3.24%
6.5	-1.70%	-3.05%	-1.80%	-2.79%	-1.97%	-2.87%
7.0	-1.49%	-2.82%	-1.56%	-2.51%	-1.69%	-2.56%

Energy capture comparisons between the hybrid truncated rotor and the thick-sharp design (Table 4.8), showed small losses in the clean condition, which were offset by significant gains in the soiled condition. Since large wind turbine blades are difficult to clean, they will operate most of the time with some degree of surface fouling. Therefore the hybrid truncated rotor appears to have a performance advantage over the thick-sharp design.

Table 4.8 Hybrid Truncated Energy Capture Comparison to Thick-Sharp Section

Wind Speed (m/s)	-2° Pitch		-1° Pitch		0° Pitch	
	Free (MWh)	Fixed (MWh)	Free (MWh)	Fixed (MWh)	Free (MWh)	Fixed (MWh)
5.5	-0.54%	2.77%	-0.59%	3.08%	-0.59%	3.57%
6.0	-0.42%	2.49%	-0.44%	2.85%	-0.40%	3.32%
6.5	-0.34%	2.23%	-0.34%	2.61%	-0.27%	3.05%
7.0	-0.28%	2.00%	-0.27%	2.39%	-0.19%	2.80%

5.0 IMPACT OF ALTERNATIVE MATERIALS

5.1 Blade Materials Evaluation Methodology

The basic concept for evaluating interesting candidate materials for wind turbine blade use was to compare their weight and cost performance when used as the spar cap material. This was done at the 50 meter blade size, using the thickest of the blade thickness distributions from the preceding parametric variation work. In Section 3.0 we examined the effects of a constant width spar cap and compared that against the baseline design. The baseline structural design has a spar cap that goes from 15% to 45% of chord, and is twice as thick at its center as at its edges, as was used in the parametric study. The thickness of the spar cap was adjusted to match the same design flapwise loading distribution, at a strain appropriate to each material, and a trailing edge spline was added as required to meet twice the edgewise deadweight bending moment at a design fatigue strain of 0.125%.

Evaluation of section properties was performed at stations 85, 65, 45, 25, and 15, with a circular tube of spar cap material at station 5 taken to represent the basic root laminate, before root buildup. Total blade shell weight and spar cap weights were computed based on these station section properties. The root tube was assumed to be composed of spar cap material for the weight calculations. While the trailing edge spline was taken to be of the same material as the spar caps for the overall weight calculations, it was a minor fraction of blade weight, and wasn't included in the spar cap weight and cost calculations. This provides a clean focus on just the primary impact on spar cap and root structure.

Note that the costs cited are only the material costs, and do not include a labor component. While labor costs are certainly significant, and may vary from material to material, assessing those differences accurately was judged to be outside the scope of this phase of the study. The relative impact of labor and material costs was previously evaluated and is documented in Reference 2.

The materials selected for comparative evaluation were E-glass, large tow carbon fiber, S-glass, and a wood/epoxy/carbon hybrid studied previously in SBIR-sponsored research by Gougeon Brothers. Inc. (GBI) [10]. In order to make these results more comparable to the recent Global Energy Concepts (GEC) study of glass and carbon [11], the composition and properties of the spar cap materials were matched to ones used by GEC. Since there were a number of variations of glass and carbon presented, it was necessary to choose which to use in this work.

Our choice was also guided by a desire to make selections that were close to the preceding parametric study, and to the material properties typically used by TPI in its blade design work. This lead to the selection of a 40% fiber volume fraction, with 80% of the unidirectional fiber aligned along the span, as the baseline for the all fiberglass and carbon/glass hybrid constructions. The properties for the wood/epoxy/carbon hybrid were those of the most heavily carbon augmented material investigated in the Gougeon SBIR work. For reference purposes we have included summary tables obtained from a reference handbook [12] for a variety of laminate types and composite reinforcing materials (Tables 5.1 and 5.2). Among the laminates compared in Figure 5.1, only glass provides both low cost and high stiffness.

Table 5.1 Properties of Different Laminates (Reference 10)

	Laminate properties									
Reinforcing fiber	Mechanical strength	Electrical properties	Impact resistance	Chemical resistance	Machining and punching	Heat resistance	Moisture resistance	Abrasion resistance	Low cost	Stiffness
Glass strands	X		X	X		X	X		X	X
Glass fabric	X	X	X	X		X	X			X
Glass mat			X	X		X	X		X	X
Asbestos		X	X			X				
Paper		X			X				X	
Cotton/linen	X	X	X		X				X	
Nylon		X	X	X				X		
Short inorganic fibers	X		X						X	
Organic fibers	X	X	X	X	X			X		
Ribbons		X					X			
Metals	X		X				X			X
Polyethylene	X		X		X					X
Aramid	X	X	X			X		X		X
Boron	X		X			X				X
Carbon/graphite	X		X			X				X
Ceramic	X		X						X	

Table 5.2 Properties of Glass Laminates (Reference 10)

	Glass type					
	A	C	D	E	R	S and S2
Physical properties						
Specific gravity	2.50	2.49	2.16	2.52–2.61	2.55	2.49
tensile strength, lb/in^2	350,000	400,000	350,000	500,000	640,000	665,000
Tensile elastic modulus	9,800,000	10,000,000	7,500,000	10,500,000	12,475,000	12,600,000
Elongation at 72°F, %	—	—	—	3–4	—	5.4
Poisson's ratio	—	—	—	0.22	—	—
Thermal properties						
Softening point, °F	1300	1380	1420	1540–1555	1481	1778
Coefficient of thermal expansion—in/in/°F × 10^{-7}	90	40	17	28–33	74	13–17
Thermal conductivity (k) BTU in/hr/ft^2/°F at 72°F	—	—	—	7.2	6.9	—
Specific heat at 72°F BTU/lb/°F	—	—	—	0.197	—	—
Optical properties						
Index of refraction	1.512	1.541	1.47	1.56	—	1.523
Electrical properties						
Dielectric constant, 72°F, 10^6 Hz	6.90	6.24	3.56	6.1–6.7	6.2	5.34
Loss tangent, 72°F, 10^6 Hz	0.0085	0.0052	0.0005	0.001	0.0015	0.002
Features						
	Soda-lime glass with limited water resistance	Chemical glass	Lowest dielectric constant	Electrical grade	High strength plus modulus	Highest physical properties
Uses						
	Surface mat	Chopped roving surface mat yarns	Yarn	Roving fabrics yarn	Yarn	Roving yarn

5.2 E-glass

E-glass is the dominant reinforcement fiber for current wind blade production. As cited in the GEC study, E-glass laminate modulus along the blade axis was assumed to be 27.1 GPa (3.93 msi), and specific gravity was taken as 1.75. These values are appropriate for a 40% fiber volume fraction with 80% of the fibers oriented in the spanwise direction. The remaining 20% of the fiber is aligned at ±45 degrees. Material cost was taken to be $4.18/kg ($1.90/lb), based on the GEC value.

Using the baseline blade geometry at a 0.45% design strain, the E-glass spar blade was found to have a total shell weight of 12,033 kg (26,473 lbs), with 7,710 kg (16,961 lbs) in the spar caps (Table 5.3). At the current estimated price of $4.18/kg ($1.90/lb), the spar cap materials cost would be $32,226. With the thick blade geometry, the E-glass spar blade was found to have a total shell weight of 10,085 kg (22,187 lbs), with 5342 kg (11,753 lbs) in the spar caps, for a spar cap materials cost of $22,331. These weight and cost figures provide the reference for the other materials to compare against, since this material selection, with its associated properties and costs, has been tied to current industry practice, within the limits of these generic blade designs.

Table 5.3 E-glass Blade Summary

	Baseline Blade			Thick-Sharp Blade		
	Weight (kg)	Weight (lb)	Cost ($)	Weight (kg)	Weight (lb)	Cost ($)
Spar Cap	7,710	16,961	$ 32,226	5,342	11,753	$ 22,331
Skin	4,323	9,512	$ 18,073	4,743	10,434	$ 19,825
Total Shell	12,033	26,473	$ 50,299	10,085	22,187	$ 42,156

5.3 S-glass

5.3.1 Design Strain

S-glass is a magnesium aluminosilicate with higher alumina content than the more commonly used E-glass. S-glass has a higher fiber modulus of 85.5 GPa (12.4 msi), versus 72.4 GPa (10.5 msi), an increase of just over 18%. Its fiber tensile strength is 4600 MPa (670 ksi) versus 3,450 MPa (500 ksi) for E-glass, an increase of over 33% [13]. Its fatigue strength is also increased. It is used in applications where a combination of high tensile strength and high strain to failure are needed, such as helicopter rotor blades. From a technical standpoint, it is an interesting material for the wind turbine rotor blade application, but relatively low volume usage has kept its price high, so it has not been a mainstream wind turbine rotor material. However, wind turbine blade manufacture is now a high enough volume market, that it was decided to see what S-glass might have to offer, particularly if that market power could drive its prices toward E-glass levels.

The fact that S-glass is not a mainstream wind turbine material has meant that it is not included in the extensive Montana State University database for fiberglass (and now carbon). A carefully controlled comparison to E-glass for the compression limit strain taken to govern the current design study therefore does not exist. In communication with John Mandell, who leads the MSU materials test work, it was suggested that the same compression limit strain as that for E-glass be used. This was done, even though data from the Owens Corning web site showed over a factor of two greater specific

compression strength (2909 vs 1187) for S-2 fiber versus E-glass, because factors such as fabric architecture and manufacturing process are known to have a dominant effect on compression strength properties. There is also the fact that deflection already limits some blade designs, so a higher material strain might not be of much practical impact. The fully factored design limit strain was thus taken to be 0.45%, as derived in the Global Energy Concepts report [11].

5.3.2 Material Cost

To keep cost values as comparable as possible to the GEC study, it was necessary to establish material cost on a similar basis. Pricing information from the Owens Corning web site indicated a current price range of $20 - $26 per kg for heavy tow carbon, and the GEC price for stitched biax or triax fabric of $23.30 per kg ($10.57/lb) was found to fall in the middle of that range. This was taken as indication that the web site range of $13 - $18 per kg for S-glass would be similarly current and comparable, and the middle of range price of $15.40 ($7.00/lb) was taken as the estimated current price for stitched biax or triax S-glass fabric. The price for woven E-glass uni was cited by GEC to be $3.60 per kg, versus $4.50/kg for the stitched material, so the cost reduction of $0.90/kg ($0.41/lb) was applied, resulting in an estimated price of $14.50/kg ($6.59/lb) woven unidirectional S-glass fabric. Using a 67% mix of woven uni with 33% stitched triax gives the 0.8 uni fraction chosen for this comparison work, with a resulting estimated current material cost of $10.43/kg ($4.74/lb), using the GEC value for epoxy cost. This compares to the estimated E-glass material cost of $4.18/kg ($1.90/lb), clearly showing the dramatic impact of the current high cost of S-glass fiber.

5.3.3 Discussion of Results

Using the thick blade geometry and a 0.45% design strain, the S-glass spar blade was found to have a total shell weight of 8527 kg (18,759 lbs), with 4380 (9635 lbs) in the spar caps. At the current estimated price of $10.43/kg ($4.74/lb), the spar cap materials cost would be $45,659. While the weight is certainly better than E-glass, the price is not competitive, given current fiber pricing. This is where market economics are felt. The process of making S-glass is quite similar to that of E-glass, but since circuit boards created a big market for E-glass in the early years, it was there that the high volume economies first occurred. Structural applications have also usually used E-glass (due to cost), even though S-glass has superior mechanical properties. As an indication of what might be possible, the spar cap cost for an S-glass blade at E-glass prices was computed to be $18,310. This is the lowest spar cap cost of the materials considered here. It may be worth the wind turbine industry investigating if it can create a sufficient market to drive down S-glass prices. This would be somewhat akin to how increased volume is currently driving down carbon prices, but the very low cost of mature E-glass production hints that the mature cost for S-glass may lie well below that for carbon, due to the different materials and processes used. This deserves further investigation, but that is beyond the scope of this phase of the current project.

5.4 Carbon/E-glass Hybrid

Price reductions for large tow carbon fiber have brought it into the range where it is now a candidate for primary wind turbine blade structure. As characterized in the GEC study, its modulus along the blade axis was taken to be 66.2 GPa (9.60 msi), and the specific gravity was assumed to be 1.52. This is for a 40% fiber volume fraction with 80% of the

fibers oriented in the spanwise direction. The remaining 20% of the fiber is E-glass aligned in the ±45 degree directions. Material cost was taken to be $11.70 per kg ($5.31/lb), based on the GEC value for current large tow carbon fiber. A second spar cap cost was computed using $8.69 per kg ($3.95/lb) as the potential cost of larger tow, next generation carbon fiber spar cap material.

Using the thick blade geometry at a 0.34% design strain, the carbon/E-glass hybrid spar blade was found to have a total shell weight of 7,300 kg (16,060 lbs), with 2895 kg (6,369 lbs) in the spar caps. These are the lowest weight values for any of the material systems studied. At the current estimated price of $11.68 per kg ($5.31/lb), the spar cap materials cost would be $33,813. At the target price for next generation large tow carbon fiber of $8.69 per kg ($3.95/lb), the spar cap materials cost would drop to $25,177.

5.5 Carbon / Wood / E-glass Hybrid

5.5.1 Design Strain

Zebrawood is a convenient name used to refer to the inclusion of carbon fiber between the layers of epoxy laminated Douglas fir, the regular black lines suggesting the "zebra" term. This concept makes dual use of the epoxy, to both bond the veneer and wet the carbon, so the weight and cost increments are not much beyond that for just the carbon fabric. Fir and carbon were known to have similar working strains, so this material received considerable study as a cost-effective way to get higher strength and stiffness wherever a wood/epoxy blade might need it. Further, it was thought that the fir could provide a measure of damage tolerance, and protection from external impact, which is often a concern for all carbon structures.

Results from the SBIR funded study by Gougeon Brothers Inc. [10] included both static and fatigue testing and were used as the basis for estimating a compression design strain for this material. The material selection portion of this study included both static and fatigue screening tests of 11 types of carbon fabric. At the time of this work in the late 1980's, carbon was much more expensive than it is now, so the fabric selected then to maximize the property improvements per unit cost would not necessarily yield the best results today.

For the purposes of exploring the impact of carbon augmented wood/epoxy laminate in the current context, the heaviest fabric tested at that time, Techniweave 12K, was selected. It is entirely possible that even heavier fabrics would be a more cost-effective choice today, but this is the heaviest reinforcement for which data is available. The Techniweave 12K reinforced Douglas fir was found to have a bulk modulus along the grain of 27.5 GPa (3.99 msi), and a weight of 47.03 lbs/ft^3, for a specific gravity of 0.754. The average compression strength was found to be 141 MPa (20.5 ksi), which gives a typical failure strain of 0.514%.

To compute a design strain, four separate factors were applied in the same fashion as was done for commercial wood/epoxy blade design. The specific factors used to account for variability (1.145), moisture (1.274), temperature (1.1), and size effect (1.122), resulted in a compression design strength of 87 MPa (11,350 psi), and strain of 0.285%. Each of these could be debated to some extent due to the limited data, but moisture and size effects, in particular, required the exercise of engineering judgement. For instance, the reduction of strength of wood/epoxy with moisture has been studied in some depth, but no

data for zebrawood exists. Should the known correction be applied to the whole strength of the specimens, or only the part due to the wood? The conservative choice of applying it to the whole strength was made, but this may overstate the strength reduction. Similarly, the known size effect correction for wood laminate in compression was applied, even though the consistent properties of the carbon may reduce the size effect correction.

While the derivation of the 0.285% compression design strain limit used well established methods for wood/epoxy blade design, there was a clear question of whether it was really comparable to the other spar cap materials, since it did not include the usual GL factors. This is not a simple question, since the wood/epoxy calculation includes specific factors for moisture and size effect that GL does not. It might be argued that these are covered in the 1.5 GL "aging" factor. On the other hand, GL includes factors for items such as synthetic material type and post-curing that do not directly apply to zebrawood. To provide an overall factor nearer the GL norm, a final design strain was derived by treating the wood/epoxy calculations with GL factors that can be established by supporting data, and then applying the 1.35 general material factor, resulting in a 0.211% design limit strain. By comparison, the value for the carbon/glass hybrid material used for this study was 0.34%, which is over 60% higher allowable strain. With further testing of a modern form of carbon/veneer material, it may be possible to establish significantly higher performance. It is known that only a few sites such as the Texas Gulf Coast have conditions that combine hot-wet to the degree represented by the chosen factors, so there is built in excess margin for typical sites. For these reasons, the chosen design strain for zebrawood in this study is viewed as more likely conservative than not.

5.5.2 Material Supply

A concern about using natural material is the available supply of suitable veneer going forward, without relying on old growth Douglas fir, which has been the traditional base veneer. This issue was addressed without complete success by Advanced Blade Mfg., with results presented in a Sandia report [14] published in 1999. The two alternatives considered were new growth fir and southern pine. Both showed promise, but did not achieve performance completely equivalent to the baseline old growth Douglas fir.

The new growth fir results in particular deserve some discussion. Strength testing showed a bi-modal character, with part of the data essentially matching the old growth fir, and another part coming up well short of expected performance. It is noted in the report:

> " … the veneer had been manufactured from quite small Douglas fir boles (6 to 10 inch in diameter) … the use of juvenile wood for production of the large veneer sheets could be a source of the veneer weakness, since heart wood is weaker than sap wood. Juvenile wood would also be more susceptible to damage during handling since the smaller logs can be more easily bent or excessively shocked by harvesting procedures. … It is believed that the weakness of the new growth Douglas fir tested was representative of the juvenile wood used to produce the veneer."

And in the conclusions:

> " … several mills were identified that are currently producing veneer from larger "second growth" Douglas fir groves (boles 16 – 30+ inch diameter).

It is very probable that veneer produced from these larger boles will not evidence the same failures as the juvenile wood did in fatigue testing."

This is a reasonable set of conclusions given the test data, particularly in view of the fact that part of the data was up to historical norms. While it remains to be proven, it is reasonable to expect that veneer of sufficient quality can be obtained from renewable sources to produce zebrawood of equivalent strength to that tested in the Gougeon SBIR report. We believe it is also possible to obtain adequate performance, as compared to the previous Gougeon test work, using materials that are cost effective for mass production of large wind turbine blades.

5.5.3 Material Cost

The Techniweave 12K material used in the Gougeon SBIR study had a cited cost of $29.08/lb. It was estimated that there would be 7.98 lbs of this material per ft^3, along with 6.44 lbs of epoxy, and 26.85 lbs of veneer. The cost of veneer at that time was $0.39/lb, and epoxy was $2.30/lb, for a total material cost per pound of $5.77. Clearly the cost was dominated by the carbon fabric, which was by far the most expensive component.

The 1999 ABM report cited new growth fir veneer price at $3.20 a sheet. Since a veneer sheet is 8 to 9 lbs, this is $0.36 to $0.40 per pound, consistent with the Gougeon study value. To obtain top quality veneer from larger new growth boles, let us assume a price escalation to $0.50/lb. In Reference 11, GEC reported a current price of $22.90/kg ($10.39/lb) for large tow carbon fabric, with a possible reduction to $15.20/kg ($6.90/lb) for next generation large tow carbon fabric. This same study cites a price of $4.60/kg ($2.09/lb) for epoxy.

To help comparisons with the GEC work, the same values for current large tow carbon fabric and epoxy will be used in the material cost calculation for zebrawood in today's market. By component, the cost contributions per pound are $0.29 for veneer, $0.29 for epoxy, and $1.76 for carbon, giving a total material cost per pound of $2.34. Clearly, this cost is dominated by the carbon component, which continues to improve, and can absorb modest increases in veneer or epoxy cost without much impact. For the near future, one would expect this price to be likely to decline, due to the cost dominance of the carbon component.

5.5.4 Discussion of Results

Using the reference blade geometry and a 0.211% design strain, the zebrawood spar blade was found to have spar caps over 2/3 of the airfoil half thickness at the 65% radial station, which puts the innermost material at extremely low efficiency levels. Some adjustment of the design via airfoil, spar cap width, or amount of carbon used locally, was necessary. It was decided to make the spar caps 50% wider at this one station, going from 10% to 55% of chord, rather than the usual 15% to 45%. With these compromises, the zebrawood spar blade shell weight was computed to be 10,184kg (22,405 lbs), with 5,785 kg (12,727 lbs) of total spar cap. At the estimated current price of $2.59, the spar cap material would then cost $32,927, dropping to $25,447 with next generation large tow carbon pricing.

5.6 Summary of Alternative Material Results

Figure 5.1 compares the blade shell weights for the four spar cap material choices. Three variations are shown for E-glass, the first for the baseline thickness distribution, the second for the thick distribution, and the third for the truncated airfoil geometry. These are at the same 0.45% design strain, as is S-glass, with carbon/glass at 0.34%, and zebrawood at 0.21%

It is evident that the thick blade distribution provides a large reduction in blade weight, with truncation providing only a small additional reduction. However, it should be kept in mind that the truncated design achieves this even though we have not include the efficiency advantage of the tapered spar cap thickness (twice as thick in the middle) of all the other designs. The zebrawood blade is similar in blade shell weight at less than half the design strain, indicating suitability for when low deflection is required. The S-glass blade achieves a significant reduction in weight below the other three, and the carbon/glass hybrid is lighter yet, even though it has lower design strain than the fiberglass blade.

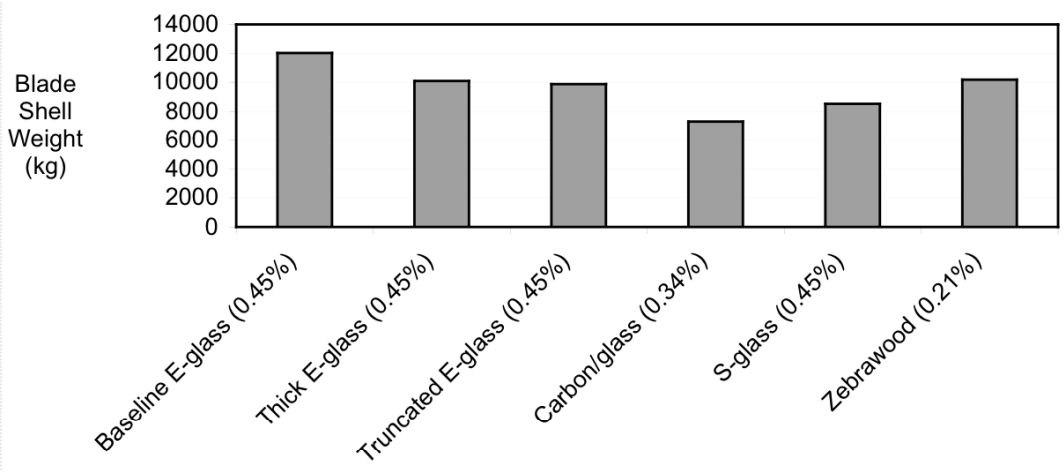

Figure 5.1 Shell Weight Comparison for Alternative Spar Cap Materials

A comparison of spar cap material costs under the equal loading is presented in Figure 5.2. The thick distribution saves approximately 30% in spar cap material costs compared to the baseline. For E-glass we assumed no reduction in material cost between current and future time periods. The carbon/glass spar cap cost is close to that for the baseline (E-glass) blade, but higher than that of E-glass with the same thickness distribution. With future next generation large tow carbon pricing, the carbon/glass hybrid closes the price gap, but is still somewhat higher. Cost for the zebrawood material is quite close to the carbon glass hybrid, both under current and future pricing scenarios. At current prices, S-glass is by far the most expensive, but if it could be reduced to current E-glass prices by large volume economies of scale, it would provide the least expensive material option under equivalent loading.

The truncated E-glass blade design uses only a little less material the thick E-glass design, and so is not shown separately. However, the constant width and thickness of its spar cap concept could provide savings in labor. If credit for freedom from ply drops could be taken, a substantial additional saving in weight and cost would be

realized in blades where fatigue at ply drops impacts the spar cap design.

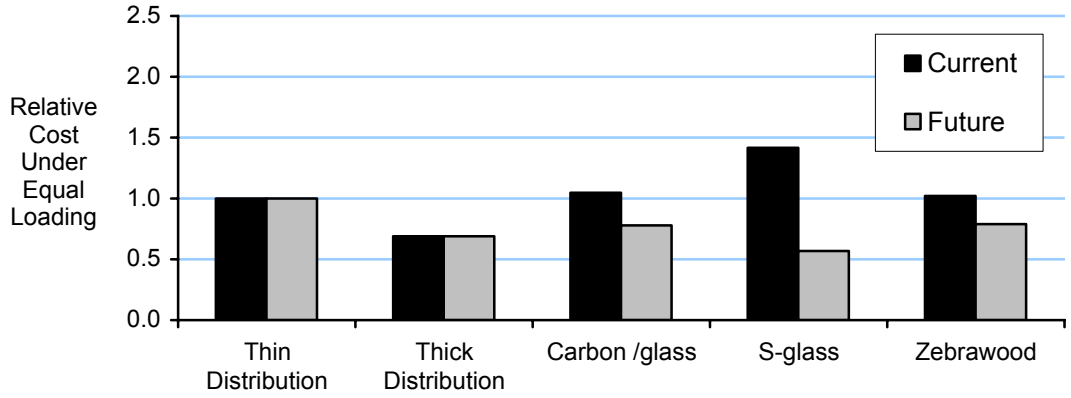

Figure 5.2 Spar Cap Cost Comparison Under Equal Loading

Figure 5.3 shows the spar cap material cost comparison assuming equal strain, as might be the case when deflection limitations require a low design strain irrespective of the spar cap material choice. The thick distribution is adopted as the new baseline in this graph, which reflects early work done at a 0.375% strain that matches none of the final study choices. Since the cost values would not be comparable to those in the preceding work, all of the values were normalized by assigning a value of 1.0 to the cost of the thick distribution with E-glass spar caps.

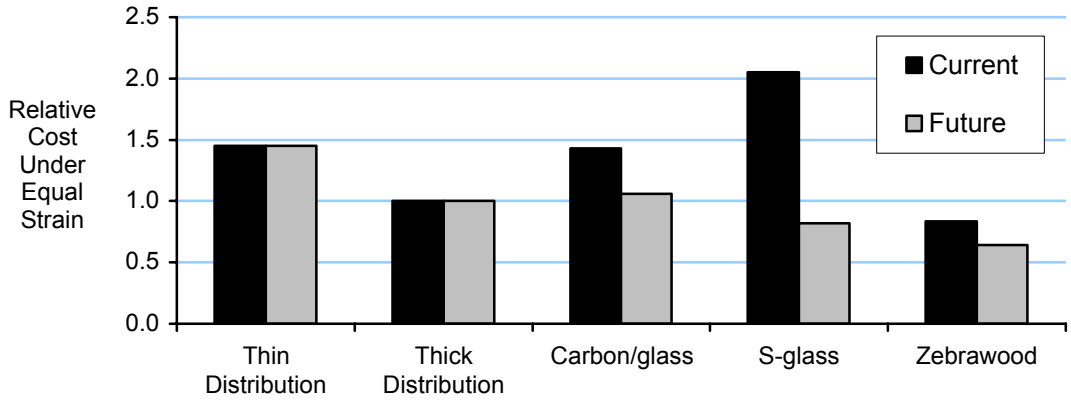

Figure 5.3 Spar Cap Cost Comparison Under Equal Strain

The carbon/glass hybrid at current prices is similar to the thick distribution E-glass cost, with future reductions based on next generation larger tow carbon bringing it down near the thick E-glass spar cap cost. S-glass is again the most expensive using current prices, but becomes very competitive if its price could be reduced to current E-glass levels. Zebrawood equals S-glass even at E-glass price, and becomes the least cost option if the future cost reductions of next generation large tow carbon material are achieved. Clearly, the level of design strain chosen will have a big impact on how these results compare, so these results should be regarded as indicative only. Still, the basic conclusion that zebrawood may be highly competitive where low strain is required appears to be valid.

6.0 IMPACT OF DESIGN CLASS

6.1 IEC Design Loads

The International Electrotechnical Commission (IEC) guidelines for wind turbine safety [15] are the primary design standard used in the wind industry. The IEC guidelines define wind sites according to a reference maximum wind speed and the mean wind speed (based upon ten minute averages), as shown in Table 6.1.

Table 6.1 IEC Wind Turbine Generator Structural Design Classes

IEC Wind Turbine Design Class	I	II	III	IV
V ref (annual 10 minute maximum, m/s)	50.0	42.5	37.5	30.0
V ave (annual 10 minute mean, m/s)	10.0	8.5	7.5	6.0

The blade design loads used in this study and in earlier work (References 1 and 2) were developed assuming IEC Class I conditions. The IEC Class I load condition was selected because it is the most structurally demanding; however, it is not necessarily representative of wind plant sites being developed currently or in the future. Most sites recently developed in the U.S. will fall within the IEC Class II or Class III designations and there is increasing emphasis on developing wind plants in IEC Class IV sites.

The IEC design guidelines stipulate an extreme gust wind speed, which occurs when the turbine is not operating. The guidelines also define a number of operating conditions which are also used to calculate design loads. In this study we assumed that the turbine tip speed and cut-out wind speed would be adjusted so that the extreme gust condition would be dominant. This assumption simplifies the analysis approach and is also a reasonable approach to optimizing turbine rotor size and specific power to specific site conditions. The blade extreme gust bending moment distributions calculated for each of the IEC load classes are summarized in Table 6.2.

Table 6.2 Blade Extreme Gust Bending Moment Distribution

Rotor Station (%)	Bending Moment Class I (kNm)	Class II (kNm)	Class III (kNm)	Class IV (kNm)
0%	20198	14593	11361	7271
10%	15763	11389	8867	5675
20%	11738	8481	6603	4226
30%	8380	6055	4714	3017
40%	5704	4121	3208	2053
50%	3640	2630	2047	1310
60%	2118	1530	1191	762
70%	1067	771	600	384
80%	415	300	233	149
90%	90	65	50	32

6.2 Impact of IEC Class on Blade Weight

Structural design calculations were performed for the thick-sharp, E-glass blade assuming the bending moment distributions provided in Table 6.2. In this analysis only the spar caps and trailing edge splines were modified. No attempt was made to account for possible reductions in skin or shear web weights. There was a significant reduction in blade weight between each IEC Design Class (Table 6.2 and Figure 6.1), especially between Class I and Class II.

Table 6.3 Thick-Sharp Blade Shell Weight as a Function of IEC Design Class

IEC Design Class	Weight (kg)	Comparison
Class I	10,085	100%
Class II	8,238	82%
Class III	7,203	71%
Class IV	5,952	59%

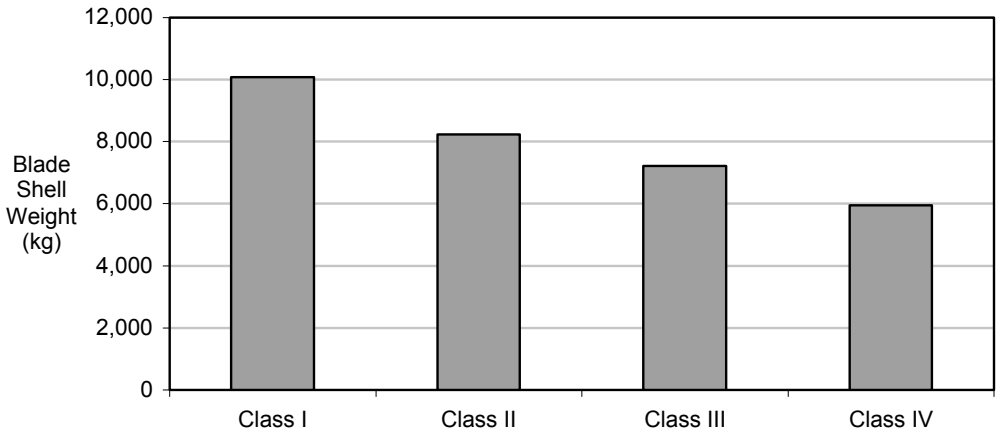

Figure 6.1 Thick-Sharp Blade Shell Weight as a Function of IEC Design Class

The impact of design class on blade cost was also significant. The change in weight between blade designs is purely due to reductions in the spar cap and trailing edge spline, with no other blade elements being changed. Therefore the change in material cost is proportional to the change in blade weight. Thus the relative cost of a Class III blade will be about 71% of a Class I design (Figure 6.2).

Some interesting trends were identified within the analysis results. The root region of the Class I blade has an 84% excess edgewise margin, which was necessary to meet the flatwise loading. This compares to a 9% edgewise margin for the Class IV design case. In a sense the flatwise and edgewise design conditions are more balanced as the wind class trends to lower wind speeds.

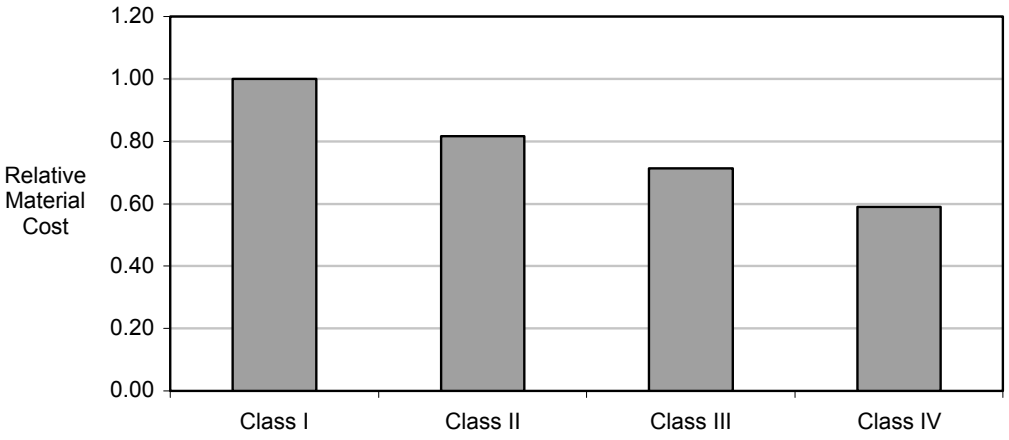

Figure 6.2 Thick-Sharp Blade Relative Material Cost as a Function of IEC Design Class

The fraction of the section weight contributed by the spar caps is reduced between Class I and Class IV. For this reason it would make sense to narrow the spar cap chordwise dimension and get a small boost in structural efficiency from using the deeper part of the section. Associated with that, one can conclude that the wider efficient structural region of the hybrid airfoils will be less beneficial for the lower wind classes. One might choose to make the inner blade a little thinner, or use more conventional airfoils.

The changes between blades designed for a given IEC Design Class are significant and that may have implications of many sorts on how an "optimized" blade will be designed. While we have not pursued the details of where that leads, its clear the overall impact on weight and total spar cap required is quite large, and that this in turn can affect many other design features. Selection of the correct design class is critical for design of well optimized blades.

7.0 CONCLUSIONS

7.1 Structural Design

The earlier parametric study effort showed that significant reductions (>15%) in blade weight and cost could be obtained by increasing inboard section thickness. This work shows that an additional 2% reduction in blade weight is possible by tailoring the inboard section shapes to maximize structural efficiency.

This study developed and applied several possible metrics for comparing structural and aerodynamic characteristics of blade sections (Table 2.1). Our work indicates that inboard sections should be weighted more strongly toward structural performance, while outboard sections are weighted most highly on aerodynamic characteristics.

This study also documents a potentially powerful method for designing the blade structure to minimize ply drops and simplify manufacturing. The concept of designing for simple structures before finalizing the aerodynamic design has not been widely applied in the wind energy industry heretofore, but the approach seems increasingly appropriate as turbines grow larger.

7.2 Performance

In addition to providing increased structural efficiency, this work has shown that the use of specially designed inboard sections will minimize and potentially eliminate performance losses as compared to conventional airfoil sections.

7.3 Materials

This study investigated several material options that could be used to reduce blade weight. Carbon/glass hybrid provides excellent weight reductions, but presents some challenges for cost and manufacturing. Additional effort should be used to investigate the cost drivers for S-glass, which could potentially provide improved strength with few manufacturing changes or risks. Further study of wood/carbon/glass hybrid (zebrawood) is warranted, as this material offers a number of benefits and appears to be cost effective.

7.4 Design Class

This study investigated the impact of IEC Design Class on the weight and cost of the blades. The results of the study show that the design class has a major impact on blade weight and cost.

8.0 REFERENCES

1. TPI Composites, “Parametric Study for Large Wind Turbine Blades”, SAND 2002-2519, Sandia National Laboratories, Albuquerque, NM, August 2002.

2. TPI Composites, “Cost Study for Large Wind Turbine Blades,” SAND report (in publication), Sandia National Laboratories, Albuquerque, NM.

3. Timmer, W.A., and van Rooij, R.P.J.O.M., "Design and Wind Tunnel Test of Airfoil DU 97-W-300," Report No. IW-98003R, Institute for Wind Energy, TU Delft, The Netherlands, March 1999.

4. Tangler, J.L., and Somers, D.M., "NREL Airfoil Families for HAWTs," NREL/TP-442-7109, NREL, Golden, CO, January 1995.

5. Timmer, W.A., "New Airfoils for Wind Turbines; a Literature Study," Report No. IW-92056RR, Institute for Wind Energy, TU Delft, The Netherlands, September 1992.

6. McGhee, R.J., and Beasley, W.D., "Low-Speed Wind-Tunnel Results for an Improved 21-Percent-Thick Low-Speed Airfoil Section," NASA TM 78650, April 1978.

7. Ladson, C.L., and Brooks, C.W., "Development of a Computer Program to Obtain Ordinates for NACA 6- and 6A-Series Airfoils," NASA TM X-3069, September 1974.

8. Drela, M., "Newton Solution of Coupled Viscous/Inviscid Multielement Airfoil Flows," AIAA Paper 90-1470, June 1990.

9. Mandell, J.F., et.al.; Fatigue of Composite Materials and Substructures for Wind Turbine Blades, Montana State University, SAND2002-0771, Sandia National Laboratories, Albuquerque, NM, March, 2002.

10. Bertelsen, W.D., and Zuteck, M.D.; “DOE/SBIR Phase 2 Report: Investigation of Fatigue Failure Initiation and Propagation in Wind-Turbine Grade Wood/Epoxy Laminate Containing Several Veneer Joint Styles”, December, 1990.

11. Griffin, D. A., “WindPACT Blade System Design Studies Task #2 Blade Study Report”, SAND report (in publication), Sandia National Laboratories, Albuquerque, NM.

12. Harper, C. A. editor; Handbook of Plastics, Elastomers, and Composites, Second Edition, McGraw-Hill, 1992.

13. Engineered Materials Handbook Volume 1 Composites”, ASM International, Materials Park, OH, 1987.

14. Poore, R. Z.; “Advanced Blade Manufacturing Project Final Report”, SAND99-2017, Sandia National Laboratories, Albuquerque, NM, August, 1999.

15. Wind Turbine Generator Systems- Part 1: Safety Requirements, Second Edition, International Electrotechnical Commission, IEC 61400-1, 1999.

DISTRIBUTION

H. Ashley
Dept. of Aeronautics and
Astronautics Mechanical Engr.
Stanford University
Stanford, CA 94305

K. Bergey
University of Oklahoma
Aero Engineering Department
Norman, OK 73069

D. Berry (5)
TPI Composites Inc.
373 Market Street
Warren, RI 02885

R. Blakemore
GE Wind
13681 Chantico Road
Tehachapi, CA 93561

C. P. Butterfield
NREL
1617 Cole Boulevard
Golden, CO 80401

G. Bywaters
Northern Power Systems
Box 999
Waitsfield,VT 05673

J. Cadogan
Office of Wind and Hydro Technology
EE-12
U.S. Department of Energy
1000 Independence Avenue SW
Washington, DC 20585

D. Cairns
Montana State University
Mechanical & Industrial Engineering Dept.
220 Roberts Hall
Bozeman, MT 59717

S. Calvert
Office of Wind and Hydro Technology
EE-12
U.S. Department of Energy
1000 Independence Avenue SW
Washington, DC 20585

J. Chapman
OEM Development Corp.
840 Summer St.
Boston, MA 02127-1533

Kip Cheney
PO Box 456
Middlebury, CT 06762

C. Christensen, Vice President
GE Wind
13681 Chantico Road
Tehachapi, CA 93561

R. N. Clark
USDA
Agricultural Research Service
P.O. Drawer 10
Bushland, TX 79012

C. Cohee
Foam Matrix, Inc.
1123 East Redondo Blvd.
Inglewood, CA 90302

J. Cohen
Princeton Economic Research, Inc.
1700 Rockville Pike
Suite 550
Rockville, MD 20852

C. Coleman
Northern Power Systems
Box 999
Waitsfield, VT 05673

K. J. Deering
The Wind Turbine Company
1261 120th Ave. NE
Bellevue, WA 98005

A. J. Eggers, Jr.
RANN, Inc.
744 San Antonio Road, Ste. 26
Palo Alto, CA 94303

D. M. Eggleston
DME Engineering
1605 W. Tennessee Ave.
Midland, TX 79701-6083

P. R. Goldman
Director
Office of Wind and Hydro Technology
EE-12
U.S. Department of Energy
1000 Independence Avenue SW
Washington, DC 20585

D. Griffin
GEC
5729 Lakeview Drive NE, Ste. 100
Kirkland, WA 98033

C. Hansen
Windward Engineering
4661 Holly Lane
Salt Lake City, UT 84117

C. Hedley
Headwaters Composites, Inc.
PO Box 1073
Three Forks, MT 59752

D. Hodges
Georgia Institute of Technology
270 Ferst Drive
Atlanta, GA 30332

Bill Holley
3731 Oakbrook
Pleasanton, CA 94588

K. Jackson (3)
Dynamic Design
123 C Street
Davis, CA 95616

E. Jacobsen
GE Wind
13000 Jameson Rd.
Tehachapi, CA 93561

G. James
Structures & Dynamics Branch, Mail Code ES2
NASA Johnson Space Center
2101 NASA Rd 1
Houston, TX 77058

M. Kramer
Foam Matrix, Inc.
PO Box 6394
Malibu CA 90264

A. Laxson
NREL
1617 Cole Boulevard
Golden, CO 80401

S. Lockard
TPI Composites Inc.
373 Market Street
Warren, RI 02885

J. Locke, Associate Professor
Wichita State University
207 Wallace Hall, Box 44
Wichita, KS 67620-0044

D. Malcolm
GEC
5729 Lakeview Drive NE, Ste. 100
Kirkland, WA 98033

J. F. Mandell
Montana State University
302 Cableigh Hall
Bozeman, MT 59717

T. McCoy
GEC
5729 Lakeview Drive NE, Ste. 100
Kirkland, WA 98033

L. McKittrick
Montana State University
Mechanical & Industrial Engineering Dept.
220 Roberts Hall
Bozeman, MT 59717

P. Migliore
NREL
1617 Cole Boulevard
Golden, CO 80401

A. Mikhail
Clipper Windpower Technology, Inc.
7985 Armas Canyon Road
Goleta, CA 93117

W. Musial
NREL
1617 Cole Boulevard
Golden, CO 80401

NWTC Library (5)
NREL
1617 Cole Boulevard
Golden, CO 80401

B. Neal
USDA
Agricultural Research Service
P.O. Drawer 10
Bushland, TX 79012

V. Nelson
Department of Physics
West Texas State University
P.O. Box 248
Canyon, TX 79016

T. Olsen
Tim Olsen Consulting
1428 S. Humboldt St.
Denver, CO 80210

R. Z. Poore
Global Energy Concepts, Inc.
5729 Lakeview Drive NE
Suite 100
Kirkland, WA 98033

R. G. Rajagopalan
Aerospace Engineering Department
Iowa State University
404 Town Engineering Bldg.
Ames, IA 50011

J. Richmond
MDEC
3368 Mountain Trail Ave.
Newbury Park, CA 91320

Michael Robinson
NREL
1617 Cole Boulevard
Golden, CO 80401

D. Sanchez
U.S. Dept. of Energy
Albuquerque Operations Office
P.O. Box 5400
Albuquerque, NM 87185

R. Sherwin
Atlantic Orient
PO Box 1097
Norwich, VT 05055

Brian Smith
NREL
1617 Cole Boulevard
Golden, CO 80401

J. Sommer
Molded Fiber Glass Companies/West
9400 Holly Road
Adelanto, CA 93201

K. Starcher
AEI
West Texas State University
P.O. Box 248
Canyon, TX 79016

A. Swift
University of Texas at El Paso
320 Kent Ave.
El Paso, TX 79922

J. Thompson
ATK Composite Structures
PO Box 160433
MS YC14
Clearfield, UT 84016-0433

R. W. Thresher
NREL
1617 Cole Boulevard
Golden, CO 80401

S. Tsai
Stanford University
Aeronautics & Astronautics
Durand Bldg. Room 381
Stanford, CA 94305-4035

W. A. Vachon
W. A. Vachon & Associates
P.O. Box 149
Manchester, MA 01944

C. P. van Dam
Dept of Mech and Aero Eng.
University of California, Davis
One Shields Avenue
Davis, CA 95616-5294

B. Vick
USDA, Agricultural Research Service
P.O. Drawer 10
Bushland, TX 79012

K. Wetzel
K. Wetzel & Co., Inc.
PO Box 4153
4108 Spring Hill Drive
Lawrence, KS 66046-1153

R. E. Wilson
Mechanical Engineering Dept.
Oregon State University
Corvallis, OR 97331

M. Zuteck
MDZ Consulting
601 Clear Lake Road
Clear Lake Shores, TX 77565

M.S. 0557	T. J. Baca, 9125
M.S. 0557	T. G. Carne, 9124
M.S. 0708	H. M. Dodd, 6214 (25)
M.S. 0708	T. D. Ashwill, 6214 (10)
M.S. 0708	D. E. Berg, 6214
M.S. 0708	P. L. Jones 6214
M.S. 0708	D. L. Laird, 6214
M.S. 0708	D. W. Lobitz, 6214
M.S. 0708	M. A. Rumsey, 6214
M.S. 0708	H. J. Sutherland, 6214
M.S. 0708	P. S. Veers, 6214
M.S. 0708	J. Zayas, 6214
M.S. 0847	K. E. Metzinger, 9126
M.S. 0958	M. Donnelly, 14172
M.S. 1490	A. M. Lucero, 12660
M.S. 0612	Review & Approval Desk, 9612 For DOE/OSTI
M.S. 0899	Technical Library, 9616 (2)
M.S. 9018	Central Technical Files, 8945-1